Title

SOME FUNDAMENTAL CONSIDERATIONS IN DESIGN OF HIGH STRENGTH METALLIC MATERIALS

Authors

Zackay, Victor F.
Parker, Earl R.

Publication Date

1964-08-01

UCRL-11588

University of California

Ernest O. Lawrence Radiation Laboratory

SOME FUNDAMENTAL CONSIDERATIONS
IN DESIGN OF HIGH STRENGTH METALLIC MATERIALS

Berkeley, California

Rept. sub. for presentation in the 2nd International Materials Symposium, Berkeley, June 1964.

Rept. sub. for pub. in the Proceedings.

UCRL-11588

UNIVERSITY OF CALIFORNIA

Lawrence Radiation Laboratory
Berkeley, California

AEC Contract No. W-7405-eng-48

SOME FUNDAMENTAL CONSIDERATIONS IN DESIGN OF HIGH STRENGTH METALLIC MATERIALS

With an Appendix by J. Friedel

Victor F. Zackay and Earl R. Parker

August 1964

UCRL-11588

SOME FUNDAMENTAL CONSIDERATIONS IN DESIGN OF HIGH STRENGTH METALLIC MATERIALS

With an Appendix by J. Friedel*

Victor F. Zackay and Earl R. Parker**

Abstract

The problem of obtaining high strength with substantial ductility is reviewed from several different viewpoints. The theoretical strength of the structural metals is first estimated and then compared with obtainable strengths. The superiority of certain metals is rationalized in terms of dislocation theory and microstructure. Several processes for increasing the strength of steel while retaining adequate ductility are described. The limitations of strength in alloy systems that undergo precipitation by heterogeneous nucleation are summarized. Further increases in strength and ductility are suggested by the utilization of phase transformations involving homogeneous nucleation.

---

* University of Paris, France

** Inorganic Materials Research Division, Lawrence Radiation Laboratory and Department of Mineral Technology, College of Engineering, University of California, Berkeley, California.

INTRODUCTION

High strength materials fall into two general classes: those that undergo some plastic flow before fracture, and those that do not. Both classes are technologically important. The basic factors that control the strength of ductile materials, however, are not the same as those that govern the fracture characteristics of brittle materials. Consequently, each class must be analyzed separately. The problem of combining strength with toughness in ductile materials will be considered herein.

Ductility and toughness in metals depends upon the behavior of dislocations. A minimum of ten percent elongation is generally considered essential for highly stressed structural materials. For satisfactory service, plastic flow must be able to redistribute the high local load around notches and other discontinuities before cracks can form. Large numbers of dislocations must be able to move substantial distances in regions of high stress concentration if notch-brittleness is to be avoided. In conflict with this requirement of notch ductility is the fact that high strength can only be obtained in ductile materials if plastic flow is inhibited by barriers that restrict the movement of dislocations. Thus, high strength and good toughness are seemingly incompatible requirements and, in general, the strongest metals tend to be brittle and the ductile ones weak. The problem of combining the two desirable properties, strength and toughness, is a difficult one to solve. The distance between dislocation barriers must be small for high strength, but the number of dislocations required for toughness must be large. Before reviewing the nature and effectiveness of dislocation barriers, the theoretical shear strength of a dislocation-free crystal will be estimated to provide a figure for the upper limit of the strength of metals.

THEORETICAL YIELD STRENGTHS

Frenkel,[1] Orowan,[2] and recently Cottrell,[3] among others, have considered the problem of estimating the theoretical shear strength of crystals. A theoretical shear strength of G/15 is assumed in this paper for body-centered cubic metals--this value being consistent with both theory and the measured strengths of iron whiskers. Since strength is customarily determined by tensile testing, the theoretical tensile strength becomes 2(G/15) or G/7.5.

Friedel (see Appendix), working on this problem with the authors, calculated the effect of dislocation splitting on the theoretical strength of the close-packed metals. He concluded that strong splitting will lower the theoretical strength by about 40 percent. Thus, for fcc and hexagonal close-packed metals having stacking fault energies (SFE) of less than 200 ergs/cm^2, i.e., Cu, Ag, and Au, the theoretical shear strength will be about G/25 rather than G/15. However, the stacking fault energies of Aℓ and Ni are so high that dislocations do not split into partials, and in this case, the theoretical shear strength remains G/15. On the basis of the above considerations it is possible to estimate the maximum attainable tensile yield strengths of the metallic elements. This has been done for a number of metals, and the results are included in the figures that will be discussed next.

COMPARISONS OF MEASURED AND THEORETICAL YIELD STRENGTHS

The maximum tensile yield strengths attained to date for the strongest alloys of ten different metals are shown in Fig. 1.* The values shown in

* MAB Report 187-M, was a primary, although not exclusive, source of the alloy strength data.

this figure were reduced to strength-to-weight ratios and replotted in Fig. 2. A more revealing comparison is obtained when the ratio of the theoretical-to-measured strength is plotted against an equivalent temperature. The latter was obtained by dividing the test temperature by the melting point (on an absolute scale). The variation of the theoretical strength with temperature was assumed to be linear from the Debye temperature to 70% of the melting point.[4]

Plots of the ratios of measured-to-theoretical strengths vs the equivalent temperatures for alloys of Fe, Ti, Aℓ, Mg, (Ni,Co) and Be are shown in Fig. 3. Theoretical strengths of G/25 were used for austenitic stainless steels and for the (Ni,Co) superalloys because these metals have stacking fault energies below about 200 ergs per square centimeter. A value of G/15 was used for the other alloys. The G/15 is appropriate for all bcc alloys and for aluminum. Stacking fault energies are not known for Mg, hcp Ti, or Be, so the proper value of theoretical strengths for these metals remains in doubt. At low values of equivalent temperature, the bcc alloys of Fe and Ti are clearly superior--each being about a third of the theoretical strength. At higher values of the equivalent temperature the fcc alloys of Aℓ and (Ni,Co) are superior. The actual strengths of commercial alloys are obviously <u>not</u> determined by the elastic moduli of the base metals. There is at present no a priori theoretical reason why the bcc alloys of Fe and Ti should be superior at low equivalent temperature.

A study of the compositions of the commercial materials reveals that the strongest bcc materials contain a substantial amount of alloying elements but no more than those having fcc structures. One of the strongest materials, namely iron, has a phase change which permits major modifications of the

microstructure by heat treatment. However, the strongest bcc titanium alloy does not. Stable phases leading to high strength can be produced in the titanium alloy by a combination of quenching, cold-working, and aging. Thus, the factors that the best materials have in common are that they both have bcc structures and they both contain elements that will form strong stable precipitates as a consequence of thermo-mechanical treatments. In the absence of evidence to the contrary, it may be assumed that any metal exhibiting substantial ductility in polycrystalline form can be made to have a high fraction of its theoretical strength. An example of such a possibility is hcp titanium, which, unlike beryllium, is ductile in spite of its hexagonal crystal structure.

A very interesting fact is revealed in Fig. 4 where measured-to-theoretical strength ratios of the low melting alloys of Mg and Aℓ with those of the refractory alloys of W, Mo, Ta, and Nb are compared on an equivalent temperature basis. When plotted in this manner, aluminum alloys are superior to the refractory metal alloys over the entire temperature range, and bcc iron is far superior to the refractory metals at temperatures below about half of the melting temperature. From this comparison it may be concluded that diligent effort in alloy development could produce significant improvements in the strengths of refractory alloys.

STRENGTHENING MECHANISMS -- LIMITATIONS AND POSSIBLE IMPROVEMENTS

The oldest and still the simplest method for increasing the yield strength of a metal is by cold work. Plastic straining below the recrystallization temperature can be used to produce a several-fold increase in the yield strength of pure metals. As extensive examinations have revealed,[5] dislocations in plastically deformed metals tend to collect in tangled networks.

The portion of the crystal inside the network is in general substantially free from dislocations, and there are no barriers in this region to inhibit the movement of slip dislocations. The distance between barriers is thus equal to the cell diameter, which reaches a limiting size during plastic flow of approximately 0.5 micron.[5] A dislocation bowing out into the nearly perfect crystallite 0.5 microns in diameter, and pinned at opposite cell walls, would move freely under a stress of only a few thousand pounds per square inch. In reality, yield stresses an order of magnitude higher result from plastic deformation. This occurs because of the fact that the dislocation sources, which are located in the tangled cell wall networks, are pinned by interactions with other dislocations. Transmission electron microscopy has shown that the pinning point spacing is of the order of one-tenth of the cell diameter. Observations indicate that it is probably not reasonable to expect pure metals or solid solutions to develop cell sizes smaller than about 0.5 micron, nor is it likely that the pinning point spacing of source dislocations can be effectively reduced. Consequently, there is an upper limit of strength that can be expected from cold working alone, and this limit has already been reached in commercial materials.

From a simple consideration of the relationship* $\tau_y = \frac{Gb}{\ell}$, or $\sigma_y = \frac{2Gb}{\ell}$ for the tensile yield, it would be necessary to have barriers only 15 to 25 atomic distances apart if the theoretical tensile yield strength of a material were to be attained (see Fig. 5). However, a material at this strength level would not have any ductility because no dislocations could move. In order to permit enough dislocation movement to provide the toughness necessary

---

* τ_y = shear yield stress, σ_y = tensile yield stress, G = the shear modulus, b = the Burgers vector, and ℓ = the distance between precipitated particles through which dislocations cannot pass.

for engineering structural uses, barriers should be several times the minimum theoretical distance apart. Thus, for steel having hard carbide particles spaced at 50 atomic distances, the tensile yield strength should be about 500,000 psi. It would seem from this analysis, that the optimum combination of strength and toughness is being closely approached by some of the ausform steels. It does not seem reasonable at this time to expect that the yield strength of steel can be increased much beyond 500,000 psi by carbide precipitation without causing a serious loss in toughness.

There is still ample room for improvement in the properties of ordinary commercial steels, however, because the low values of 35,000 to 70,000 psi for the yield strengths of common structural steels leaves much room for improvement, and even the best of the conventionally treated steels, with yield strengths generally below 250,000 psi, are still weak in comparison with attainable maximum theoretical strength levels. Exploration of ways and means for producing high yield strengths, combined with good ductility and adequate notch toughness, are therefore appropriate. Two examples of research of this kind are cited in the following section.

METHODS FOR INCREASING THE YIELD STRENGTH OF HIGH STRENGTH STEELS

Iron base materials have had by far the greatest attention paid to them because of their low cost and extensive usage. Their position near the top of the list is therefore not surprising. Nevertheless, it is essential to understand the reasons for their high strength. The strongest steels are those that have been ausformed and, although results of detailed studies of this class of steels will be presented in a separate paper, an important point to note here is that plastic deformation forms an essential part of the

technological processing involved in developing superior strength. It is clearly evident from microstructure studies and from investigations of kinetics of aging that the deformation does two things: It provides closely spaced nucleation sites on which stable compounds or clusters can form, and secondly, plastic flow is thought to accelerate diffusion of substitutional elements so that they can participate in the formation of finely dispersed precipitates at temperatures that are too low to cause overaging.

The maraging steels, although not as strong as the ausform steels, are also superior materials. The strength of these alloys seems to be due to the presence of a finely dispersed precipitate. Additional benefits can be derived in the maraging steels by following the practice employed in ausforming, which consists of plastically straining the austenite prior to the phase transformation.(6)

Among the strongest class of materials are the body-centered cubic titanium alloys, which also derive their strengths from a combination of factors similar to those that produce superior steels. Although there is no phase transformation in these alloys, cold working plus aging promotes the formation of a finely dispersed precipitate. The well-known B120VCA alloy is superior for this reason.

Two extensions of alloy treatment have been made by the authors and their co-workers. One of these consists of transforming a small amount of the austenite in an alloy steel by cooling just below the M_s temperature, and then reheating to an intermediate temperature to temper the martensite, followed by a series of similar treatments wherein the remaining austenite is transformed in stages, with intermediate reheatings, until, after about ten or so cycles, all the austenite has been transformed. This treatment has the effect of producing a very fine microstructure. The martensite plates are prevented from growing to large sizes because of the presence of previously transformed

material. Figure 6 shows the heat treating cycle employed, and Fig. 7 shows the corresponding hardness at each stage of treatment. Figures 8 through 10 are photomicrographs that show the structure for several stages of the treatment.

Another interesting and potentially useful extension of the principles involved is the use of small amounts of plastic deformation, followed by aging at an intermediate temperature, to increase the strength of quenched and tempered alloyed steels. This treatment can be applied to both conventionally treated alloy steels and to ausform steels. When ausform steels are strained at either room or slightly elevated temperature and then aged, there results a substantial increase in yield strength. This effect is illustrated in Fig. 11. It is apparent that by combining the two processes of ausforming and elevated temperature strain aging, yield strengths approaching 400,000 psi with elongations of nearly 10 percent can be achieved. One important feature is that the stress-strain curve retains a desirable and useful shape. The effect of post-tempering temperature on the strength and ductility of an ausform steel is shown in Fig. 12. All specimens were pretempered at 500°F, strained two percent at 300°F at a strain rate of 0.05 per minute. Unlike ordinary steels in which strain aging increases the strength but usually reduces ductility, as shown in Fig. 13, the strain aged ausform steels retain excellent ductility. It has been found possible to improve conventionally treated alloy steels in a similar manner. Room temperature deformation cannot normally be used for such materials because of the adverse effect of strain aging on the ductility.[7] Yount[8] has recently shown, however, that if the amount of strain is 0.4 percent or less, strengthening results without a loss of ductility. If, as in the present work, the

straining is carried out at an elevated temperature, the usual deleterious effects on elongation are significantly less and good properties result, as Fig. 14 shows.

The effect of prestrain temperature on the strength and ductility of ausform and conventional steels is shown in Fig. 15. All specimens were pretempered and post-tempered at 900°F, strained two percent at a strain rate of 0.5 per minute. It appears from the results that straining at the higher temperatures permits new and very effective barriers to form possibly because of the strain-enhanced diffusion of the solute elements.

A brief review of the processes of hardening that could contribute to the strength of an age hardening alloy may be helpful in introducing the next subject--the problem of obtaining homogeneous nucleation of a precipitate having the characteristics required to impart maximum strength.

One of the major problems encountered in precipitation hardening systems is the occurrence of heterogeneous nucleation. Nucleation tends to occur most easily at lattice imperfections or discontinuities producing precipitates preferentially at grain boundaries or at widely dispersed lattice sites. The finer, more uniform dispersion of precipitates needed for very high strength should come from a homogeneously nucleated precipitation reaction. There is one class of alloy systems in which homogeneous nucleation is known to occur, and that is alloys with miscibility gaps. The spinodal transformation, which often occurs in such alloy systems, provides homogeneous nucleation sites that can be used for the purpose of increasing strength. In most systems of this kind, however, the two phases that ultimately precipitate are usually solid solutions which make no significant contribution to strength. There are certain cases, however, wherein one of the phases can

be made hard by converting it into either an ordered structure, or, by means of a third element, into an intermetallic compound, and alloys of this kind are worthy of further investigation.

AGE HARDENING ALLOYS

There are several ways in which precipitates can act as barriers to dislocations. They can act as strong, impenetrable, noncoherent particles, or they can act as coherent or incoherent particles through which dislocations can pass, but only at stress levels much above those required to move dislocations through the parent lattice. The only sound theoretical model for the strong incoherent particle case is that of Orowan,[9] which is as follows:

$$\tau_y = \tau_s + \frac{Gb}{4\pi(d-2r)} \frac{2\phi}{} \ln \frac{d-2r}{2b}$$

where τ_y is the shear stress at yielding, τ_s is the yield stress of the matrix, G is the shear modulus, b is the Burgers vector, d is the particle spacing, r is the particle radius, and $\phi = \frac{1}{2}\left(1 + \frac{1}{1-\mu}\right)$, where μ is Poisson's ratio. The best support for the Orowan theory is the work of Ashby[10] who performed tests on internally oxidized binary alloy single crystals of copper containing silicon, aluminum and beryllium. The oxide particle size was determined by extraction replication and electron microscopy. The spacing could be calculated from the composition and the particle size. A summary of Ashby's results was published by Kelly and Nicholson.[11] The important data are reproduced in Table I.

Table I

Comparison of Measured and Calculated Yield Stresses for Internally Oxidized Alloy Copper Single Crystals[10]

Alloy, wt %	Particle Radius, Å	Particle Spacing, Å	Yield Strength at 77°K, dynes/cm²		Yield Strength at 293°K, dynes/cm²	
			Measured	Calc.	Measured	Calc.
0.3 Si	485	3000	3.4×10^8	3.3×10^8	2.5×10^8	3.08×10^8
0.25 Aℓ	100	900	8.0×10^8	11.2×10^8	6.4×10^8	10.5×10^8
0.34 Be	76	450	15.7×10^8	20.7×10^8	11.2×10^8	19.4×10^8

For the silicon alloy (which had spherical particles as assumed for calculations of interparticle spacing) the agreement between the measured and calculated values is excellent at 77°K. In the aluminum and beryllium alloys, the particles were not spherical and the measured values were about 25 percent lower than those predicted from theory. All of the measured yield strengths at room temperature were significantly below the calculated strengths. Ashby[10] suggested that at the higher temperature cross-slip occurred and that this was equivalent to increasing the interparticle distance. Other evidence in support of the Orowan theory has been summarized by Kelly and Nicholson.[11] It seems reasonably certain that this theory is valid for the case of uniformly dispersed strong spherical particles, and that measured and calculated yield strengths may be expected to agree within a factor of two. Greater differences than this may occur for several reasons, particularly when the particles are not spherical, when extensive cross-slip occurs, or when the yield strength is measured at a strain that is not near zero. Alloys containing strong particles strain harden very rapidly because slip dislocations leave dislocation rings around particles that they pass, and the effective interparticle spacing decreases rapidly as the number of rings increases.

For coherent precipitates, the passage of a dislocation leaves the material substantially unchanged because the slip dislocations pass through the particles and not around them. In this case, the rate of strain hardening is low.

Factors other than interparticle spacing govern the yield strength when slip dislocations pass through the particles. In general, the atomic arrangement within the particle will tend to be ordered, and slip will locally destroy this order. The energy necessary to disorder a unit area, γ_o, must be supplied by the external force pushing the dislocation through the particle. If there are n particles per unit of area of the slip plane, and the average radius of the particles is r, then the disordering energy is given by*

$$n\pi r^2\gamma_o$$

When a particle is sheared, the surface area of the particle is increased by approximately 2rb, where b is the Burger's vector. If the surface energy of the particle is γ_s, then the increase in surface energy per particle is $2rb\gamma_s$, and the total energy increase for n particles is

$$n\ (\pi r^2\gamma_o + 2rb\gamma_s)$$

The load per unit of area, τ, times the distance moved, b, can be equated to the internal work required, so

$$\tau = \frac{n}{b}\ (\pi r^2\gamma_o + 2rb\gamma_s)$$

The precipitate occupies a fraction, f, per unit of area, or $f = \frac{2\pi}{3} r_o^2 n$.

Substituting for n, $$\tau = \frac{f\gamma_o}{b} + \frac{\sqrt{6}}{\pi}\frac{f\gamma_s}{r_o}$$

---

*In general, the slip plane will not pass through the center of a spherical particle because it may intersect the sphere at any section. In this case the effective radius becomes the average radius, r, of circular sections, which is equal to $\sqrt{2/3}\ r_o$, where r_o is the particle radius.

If γ_o is much greater than γ_s, then the flow stress is approximately equal to $f\gamma_o/b$, and depends only on the volume fraction of precipitate and not upon the particle size.

There are various other factors that must be considered, such as the fact that the modulus of elasticity of the precipitate may differ from that of the matrix, and the energy of a dislocation depends upon the modulus. Also, because of differences in atomic volume, there may be a hydrostatic interaction between a slip dislocation and a precipitate.[12]

One of the earliest theories, due to Mott and Nabarro,[13] considered precipitation hardening from the point of view of long-range internal stresses arising from the difference in the atomic volume, δ, of the matrix and precipitate atoms. They evaluated the case for a spherical coherent precipitate of radius, r_o, which contained material having an atomic volume equal to $(1 + \delta)$[3] where the atomic volume of the matrix was unity. In this case, the stress in the precipitate is a hydrostatic pressure given by

$$P = 3K\,(\delta - \epsilon)$$

where

$$\epsilon = \frac{3K\delta}{3K + 2E/(1-\mu)}$$

K is the bulk modulus of the precipitate, E is Young's modulus of the matrix, and μ is Poisson's ratio of the matrix. The matrix is subjected to a shear strain, θ, which varies in magnitude with the distance from the particle according to the expression

$$\theta_r = \frac{\epsilon r_o^3}{r^3}.$$

The shear strain, θ_{r_o}, at the surface of the particle is independent of the radius, r_o, of the particle. Mott and Nabarro computed a mean shear strain, θ, by assuming a value of r corresponding to the average distance from a point in the matrix to the nearest particle. This is half the distance between

particles, or $\frac{1}{2}(N)^{-\frac{1}{3}}$, where N is the number of particles per unit of volume. Then

$$\theta = 8\epsilon\, r_o^3 N.$$

The volume fraction of the precipitate is

$$f = \frac{4}{3}\pi r_o^3 N$$

So

$$\theta \approx 2\epsilon f.$$

Thus, the average shear strain in the matrix is independent of the size of the particle and so is the critical stress for flow, τ_c, because

$$\tau_c \approx 2G\epsilon f.$$

This relationship applies when the interparticle spacing, d, is small enough so that Orowan looping does not occur. In this case, it is the volume fraction of precipitate, and not the interparticle spacing, that controls the yield strength.

Ductility considerations also indicate that high strength combined with toughness requires a large volume fraction of a coherent precipitate. Incoherent precipitates have large surface energies. When dislocation loops form around such particles, cracks are likely to form along the high energy interfaces because of the local stress concentrations due to the dislocation loops. The smaller the particles, the higher the local stresses and the more likely cracks are to form. This type of crack nucleation is avoided when dislocations can pass through the particles. With coherent precipitates, high local stresses are avoided, as are high rates of work hardening, and extensive plastic flow can occur at high stress levels before cracking begins.

Other factors being equal, a large volume fraction of coherent precipitate seems to be the best means for combining high strength and good toughness. Of the two main types of precipitation reactions, nucleation and

growth transformations, and spinodal decomposition, the latter seems more desirable. This phenomenon is worthy of special study.

SPINODAL DECOMPOSITION

Spinodal decomposition of a supersaturated solid solution occurs by a nucleation and growth process, but differs in that the "precipitate" is coherent with the matrix and surface energy is not involved in the formation of a stable nucleus as it is in the normal precipitation process (assuming that there is no mismatch in lattice parameters at the interface). In the theory proposed by Borelius,[14] the rate of precipitation from a supersaturated solid solution is dependent upon the sign of the second derivative of the free energy with respect to the composition. When local composition fluctuations occurring in the matrix are associated with a decrease in free energy, precipitation tends to proceed. The free energy of mixing, ΔG, is the thermodynamic factor involved. Whenever $d^2\Delta G/dx^2 < 0$, even small compositional fluctuations cause a decrease in free energy and thus become stable regions that continue to grow. Conversely, local regions that have composition fluctuations such that $d^2\Delta G/dx^2 > 0$, are associated with an increase in free energy and will thus tend to be unstable and to redissolve. The application of this principle is illustrated in the upper part of Fig. 16. The upper figure shows a solubility gap, in this case in the gold-platinum system, and the corresponding free energy of mixing curve (in terms of $\Delta G/R$) vs composition is shown in the lower figure. The spinodal region is within the dotted lines in the phase diagram. The limits of this region are set by the concave downward part of the free energy-composition curve shown in the lower figure, at the compositions corresponding to the requirement

$d^2\Delta G/dx^2 < 0$. For an alloy having an average composition at the midpoint of the solubility gap, small local composition fluctuations are more likely to occur than large ones, and so spinodal decomposition is favored over the normal kind of nucleation and growth, which requires large local compositional fluctuations to form stable nuclei. This is illustrated in the lower part of Fig. 16, where composition fluctuations A_1 and B_1 (from the average value, x) would be sufficient to start spinodal decomposition of a supersaturated solid solution, whereas large composition fluctuations, such as those shown at A_2 and B_2 would be necessary to form stable nuclei of the normal type.

Age hardening in spinodal alloys can be very effective, even in such simple systems as the gold-platinum alloys. Fig. 17 shows the hardness increases measured by Van der Toorn[15] for polycrystalline specimens of several compositions. Not only is the rate of hardening extremely rapid in alloys that undergo spinodal decomposition, but large increases in hardness may also be obtained.

Many alloys undergo spinodal reactions. Figures 18 and 19 illustrate two of the kinds of microstructures that can be obtained in such materials. A concentration of effort on such alloys may yield new materials with desirable combinations of high strength and toughness.

SUMMARY

The maximum tensile yield strengths attained to date for alloys of ten common metals have been compared with theoretically attainable values of yield strength. The best materials available at present are alloys of body-centered iron and titanium, which exhibit about one-quarter of their theoretical maximum yield strengths at room temperature. The room temperature yield

strengths of other types of alloys fall below these two materials. The alloys of the refractory metals are particularly poor when compared to other metals on an equivalent temperature scale.

A new processing technique has been developed for improving the yield strength of commercial steels. With this process, the yield strength of ausformed H-11 steel has been raised from 340,000 psi to about 400,000 psi, without serious reductions in the elongation. Another new treatment, not yet fully explored, is based on the cyclic conversion of austenite to martensite. It has been used to produce a significant increase in the hardness of a special alloy steel.

Precipitates resistant to dislocation motion must be present in bulk material if high strength is to be attained. The contributions to strength by various kinds of precipitates are discussed from a theoretical point of view, and comparisons are made between theoretical and measured yield strengths. High rates of strain hardening are to be expected with incoherent precipitates, and microcracks are expected to form at low strains in alloys containing such precipitates. Both theory and experiment lead to the conclusion that the best combination of high strength and good ductility is to be expected from alloys containing coherent precipitates through which slip dislocations can pass, but only at high stress levels.

The yield strength is dependent upon the volume fraction of the [illegible] precipitate, and a fine dispersion is essential for toughness and ductility. The spinodal decomposition reaction is ideal for producing the best type of precipitate, and examples of its effectiveness as a strengthening mechanism are cited.

Acknowledgments

The concepts and the experimental data presented in this paper form the basis of a graduate student research program initiated in the fall of last year in the Department of Mineral Technology, College of Engineering. Efforts were directed toward achieving high strength in complex solids without sacrificing too much ductility and toughness. The authors thank the following graduate students for their contributions: Steve Antolovich, Raymond Busch, Ray Carpenter, Shelley Dahlgren, David Dickson, Virendra Goel, David Porter, K. V. Ravi. This work was performed under the auspices of the U. S. Atomic Energy Commission through the Inorganic Materials Research Division of the Lawrence Radiation Laboratory.

Figure Captions

Fig. 1 Maximum measured tensile yield strengths, shown as a function of temperature, for the common metals.

Fig. 2 Maximum measured ratios of tensile yield strength-to-weight, shown as a function of temperature.

Fig. 3 Maximum measured tensile yield strength divided by the theoretical maxima, shown as a function of the equivalent temperature for the metals Ti, Fe, Aℓ, Mg, (Ni, Co) and Be.

Fig. 4 Maximum measured tensile yield strength divided by the theoretical maxima, shown as a function of the equivalent temperature for the metals Aℓ, Mg, (Ni, Co), W, Mo, Ta and Nb.

Fig. 5 Plot of theoretical tensile yield strength vs ratio of particle spacing (ℓ) and Burgers vector (b), for Orowan type hardening (i.e., $\tau_y = \frac{Gb}{\ell}$).

Fig. 6 The heat treating cycle employed in the conversion of cold-worked austenite to martensite. The schematic inserts suggest the manner in which the austenitic microstructure is converted to fine-grained martensite by alternate cycling between cryogenic and tempering temperatures.

Fig. 7 The variation of hardness with quenching temperature for several levels of cold-working. Each quenching treatment is followed by tempering at 914°F for ten minutes.

Fig. 8 Micrograph of the as-rolled austenite, X 100. Some isothermal decomposition can be seen in the grain boundaries.

Fig. 9 Micrograph of the same as-rolled austenite after several cycles of treatment at cryogenic and tempering temperatures, X 100.

Fig. 10 Micrograph of the same as-rolled austenite after completion of the cyclic treatment, X 100. Sample is virtually 100% martensite.

Fig. 11 Stress-strain curves of an ausform H-11 steel in the quenched and tempered condition (left panel) and in the quenched and tempered plus elevated temperature strain-aged condition (right panel).

Fig. 12 The effect of post-tempering temperature on the strength and ductility of an Ausform H-11 steel. All specimens pretempered at 500°F, strained two percent at 300°F at a strain rate of 0.05 per minute.

Fig. 13 Typical stress-strain curves of a quenched and tempered and a quenched, tempered and strain-aged martensitic steel.

Fig. 14 Stress-strain curves of a conventional H-11 steel in the quenched and tempered condition (left panel) and in the quenched and tempered plus elevated temperature strain-aged condition (right panel).

Fig. 15 The effect of prestrain temperature on the strength and ductility of Ausform and conventional H-11 steels. All specimens pretempered and post-tempered at 900°F, strained two percent at a strain rate of 0.5 per minute.

Fig. 16 Phase diagram and free-energy vs composition curves for the Au-Pt system.

Fig. 17 The variation in hardness with time for several alloys in the Au-Pt system after reacting in the spinodal region. From the work of Van der Toorn.(15)

Fig. 18 Transmission electron micrograph of Fe-Cu-Ni spinodal precipitate. From the work of Tufton and Nicholson.(16)

Fig. 19 Photomicrograph of over-aged (1000°C) spinodal precipitate (Ni_xAl_y) in the Al-Cu-Ni system, x 1000. From the work of W. O. Alexander.(17)

References

1. J. Frenkel, Z. Phys. 37, 572 (1962).
2. E. Orowan, private communication to A. H. Cottrell; see, Dislocations and Plastic Flow in Crystals, A. H. Cottrell, Oxford, 1953, p. 9.
3. A. H. Cottrell, vide supra.
4. Materials Advisory Board, National Academy of Sciences, National Research Council, Washington, D. C., Report MAB-187-M.
5. J. E. Bailey, Electron Microscopy and Strength of Crystals, ed. G. Thomas and J. Washburn, Interscience Publishers, New York, 1963, p. 535.
6. R. H. Bush, "Mechanical Properties of an Ausformed Maraging Steel," Trans. ASM, 56, 885 (1963).
7. E. T. Stephenson and M. Cohen, "Effect of Prestraining and Retempering on AISI Type 4340," Trans. ASM, 54, 72 (1961).
8. R. Yount, "Mar-Straining Strengthens Steels," Materials in Design Engineering, p. 68, July 1963.
9. E. Orowan, Symposium on Internal Stresses in Metals and Alloys, Institute of Metals, 1948, p. 451.
10. M. F. Ashby, Ph.D. Thesis, Cambridge University, 1961.
11. A. Kelly and R. B. Nicholson, "Precipitation Hardening," Progress in Material Science, 10, 360 (1963).
12. R. L. Fleischer, "Solution Hardening by Interaction of Impurity Gradients and Dislocations," Acta Met., 8, 32 (1960).
13. N. F. Mott and F. R. N. Nabarro, Proc. Phys. Soc., 52, 86 (1940)
14. G. Borelius, Ann. Phys. Lpz., 20, 57 (1934); Ann. Phys. Lpz., 24, 489 (1935); Ann. Phys. Lpz., 28, 507 (1937); Ann. Phys. Lpz., 33, 517 (1938); Ark. Mat. Astr. Fys., 32A, No. 1,(1945).
15. L. J. Van der Toorn, "Precipitation in Gold Platinum Alloys-II," Acta Met., 8, 715 (1960).

16. P. J. Tufton and R. B. Nicholson, Proceedings of the Fifth International Congress for Electron Microscopy, Vol. 1, CC9, Academic Press, 1962; also shown in Prog. Mat. Sci., 10, No. 3, 226 (1963).

17. W. O. Alexander, "Copper-Rich Nickel-Aluminum-Copper Alloys. Part II - The Constitution of the Copper-Nickel-Rich Alloys," J. Inst. Metals, 63, 163 (1939).

Appendix

INFLUENCE OF SPLITTING ON THE THEORETICAL ELASTIC LIMIT

J. Friedel

The purpose of this note is to point out that in crystals where dislocations are strongly split the theoretical elastic limit should be notably lowered by a factor of about $\frac{1}{2}$.

Frank's initial analysis[1] for perfect dislocations is first recalled and discussed.

1. Thermal Nucleation of Perfect Dislocation Loops

A circular loop of radius, r, and Burgers vector, b, has, under an applied (resolved shear) stress σ, an energy

$$U_v(\sigma,r) = 2\pi r \frac{Gb^2}{2\pi K} \ln \frac{2r}{b_0} - \pi R^2 \sigma b,$$

where $b_0 \simeq b$ is a parameter related to the crystal structure, and K a numerical factor between 2/3 and 1.

For increasing radii, r, U_v goes through a maximum $U_v(\sigma, R)$ for $r = R$ such that

$$0 = \partial U_v/\partial R = 2\pi \frac{Gb^2}{4\pi K} \ln \left(\frac{2R}{b_0} + 1\right) - 2\pi R\, \sigma b.$$

Hence an activation energy

$$U_v(\sigma\, R) = \frac{Gb^2 b_0}{8K} \frac{2R}{b_0} \left(\ln \frac{2R}{b_0} - 1\right) \qquad (1)$$

with

$$\sigma(R) = \frac{Gb}{2\pi K b_0} \frac{b_0}{2R} \left(\ln \frac{2R}{b_0} + 1\right) \qquad (2)$$

These equations define the activation energy U_v as an implicit function of the applied stress σ (Fig. 1).

Thermally activated nucleation can then occur in the volume or at the surface of the crystal. The second process will be shown to be slightly easier.

a. Volume activation: The strain rate, $\dot{\epsilon}$, can be estimated, assuming that each loop sweeps through the cross section A of the crystal:

$$\dot{\epsilon} = NAb \frac{\nu b^2}{\pi R^2} \exp [- U_v(\sigma)/kT],$$

where $N \simeq b^{-3}$ is the number of possible nucleation sites, and ν the Debye frequency. $\nu b^2/\pi R_1^2$ is then an estimate of the probability for the $\pi R^2/b^2$ atoms, on the area swept by the loops of radius R, to vibrate in the same direction.

This requires an activation energy

$$U_v(\sigma) = kT \ln \left(\frac{A\nu}{\pi R^2 \dot{\epsilon}}\right).$$

For T = 300°K, $\dot{\epsilon} = 10^{-4}$ sec^{-1}, R = 2b (see below) and A = 1 cm^2, this gives U_v = 1.8 e.v.

With average values $b_0 = b$, Gb^3 = 5 eV and K = 5/6, equations (1) and (2) give R = 2.2b and

$$\sigma_v = \frac{G}{9.5}.$$

This value does not depend much on the size of the crystal: for a whisker one micron thick, thus A = 10^{-8}cm^2, one finds U_v = 1.3 eV and $\sigma_v = \frac{G}{8.5}$. The value of σ_v is also little sensitive to the value taken for Gb^3, because of the steep slope of the curve, Fig. 1. The value of σ_v is however directly proportional to b/b_0, thus to take $b = b_0$ is one of the most critical approximations.

b. Surface nucleation: If a loop is nucleated at an atomically smooth surface, one needs creating only a critical semicircle of radius R, requiring half the energy $U(\sigma)$. This result assumes that the half loop does not create any surface step, i.e., its Burgers vector is parallel to the surface. The frequency factor is then reduced in the ratio of at least b/L, where L is the size of the crystal:

$$\dot{\epsilon} \leq N \frac{b}{L} A\, b\, \frac{\nu b^2}{\pi R^2} \exp\left(-\frac{U_v}{2kT}\right).$$

The activation energy required is therefore

$$U_s = \frac{1}{2} U_v \geq kT \ln\left(\frac{A\nu b}{\pi R^2 \dot{\epsilon} L}\right).$$

This gives $\frac{1}{2} U_v(\sigma) \geq 1.35$ eV for macroscopic crystals (L = 1 cm), hence, a value practically identical to that for volume nucleation:

$$\sigma_s \geq \frac{G}{10}$$

($\sigma_s \geq \frac{G}{9.5}$ for whiskers).

On the other hand, the nucleation could be definitely easier on a surface containing many steps of atomic height parallel to the slip planes of the loops. This is because the creation of a loop with a suitable Burgers vector can suppress the step over the length 2r (Fig. 2). The energy required is then

$$U_R(\sigma,r) = \frac{1}{2} U_v(\sigma,r) - 2\, r\, \gamma_s\, b.$$

This leads to an activation energy

$$U_R(\sigma,R) = \frac{1}{2} U_v(\sigma,R) - R\, \gamma_s\, b$$

with

$$\sigma_R(R) = \sigma_v(R) - \frac{2\gamma_s}{\pi R}.$$

The implicit function $U_R(\sigma)$ defined by these two equations is plotted in Fig. 1 for the likely value $\gamma_s = Gb/20$ for the surface energy of a step.[2] In the

most favorable conditions, the distances d between steps, Fig. 2, are of atomic dimensions. For such atomically rough surfaces, the same value, $U_R = 1.35$ eV, should apply as for smooth surfaces, leading to

$$\sigma_R \geq \frac{G}{15} .$$

2. Partial Dislocation Loops

For a partial (Shockley) dislocation loop of Burgers vector b' and stacking fault energy γ, the energy is

$$U'_v(\sigma,r) = 2\Pi r \frac{G(b')^2}{4\Pi K} \ln \frac{2r}{b'_0} + \Pi r^2 (\gamma - \sigma b').$$

The same reasoning as for a perfect dislocation loop gives an activation energy

$$U'_v(\sigma,R') = \frac{G(b')^2 b'_0}{8K} \frac{2R'}{b'_0} \left(\ln \frac{2R'}{b'_0} - 1\right)$$

with an activation radius R' such that

$$\sigma(R') = \frac{\gamma}{b'} + \frac{Gb'}{2\Pi K b'_0} \frac{b'_0}{2R'} \left(\ln \frac{2R'}{b'_0} + 1\right)$$

Hence, a similar discussion applies, except that b is replaced by b' and a term γ/b' is added.

a. Change of b into b': In the FCC or CPH structures, $(b')^2 = \frac{1}{3} b^2$. If one takes $b'_0 = b'$, this gives $G(b')^3 \simeq 1$ eV.

For volume nucleation, one then finds $U'_v(\sigma) = 1.8$ eV, thus $R' = 2.8\ b$ and

$$\sigma'_v = \frac{G}{16} .$$

Very similar values are obtained for surface nucleation on atomically smooth surfaces ($\sigma'_s \geq G/18.5$) and for whiskers. For surface nucleation on atomically rough surfaces, an argument similar to the one for perfect loops leads to

$$\sigma'_R \geq \frac{G}{25} .$$

b. Stacking fault energies: From the previous equations, a partial dislocation is nucleated preferentially to a perfect dislocation if

$$\gamma < \left(\frac{G}{9.5} - \frac{G}{16}\right) b^1 \simeq \frac{Gb}{50}$$

for volume nucleation in macroscopic crystals with FCC or CPH structures. Similar values obtain for whiskers or surface nucleations. Typically, $Gb/50 \simeq 200$ e/cm^2.

Thus:

1) Splitting lowers the elastic limit, σ, only if $\gamma < \frac{Gb}{50} \simeq 200$ e/cm^2, e.g., for Cu, Ag, Au, not for Al or Ni.

2) As soon as $\gamma \ll Gb/50$, the influence of the stacking fault is negligible and the splitting should lower the elastic limit by a factor near to 1/2 (9.5/16 for volume nucleation, 10/18.5 for surface nucleation on smooth surfaces, 15/25 for surface nucleation on rough surfaces). This should typically apply to Cu, Ag, Au.

3) Other factors, such as the presence and direction of surface steps of atomic height and, thus, the crystalline orientations of the surfaces should be equally important.

References

1. F. C. Frank, "The Nature of the Real Crystal," Inst. of Metals J., 86, 581-586, (1956-57).

2. J. Friedel in Les Dislocations, Gauthier-Villars, Paris, 1956, p. 198.

Titles of Figures

1. Activation energy U as a function of the applied stress σ for the nucleation of a perfect loop.
   V: volume nucleation; $U = \frac{8K}{\mu b^2 b_0}$ Uv and $\sigma = \frac{2\pi K b_0}{\mu b}\sigma$.
   S: surface nucleation; $U = \frac{16K}{\mu b^{1} 2 b_0^1}$ U_R^1 and $\sigma = \frac{2\pi K b_0}{\mu b}\sigma$.

2. Nucleation of a loop on a surface containing many steps of atom height parallel to the slip planes of the loops.

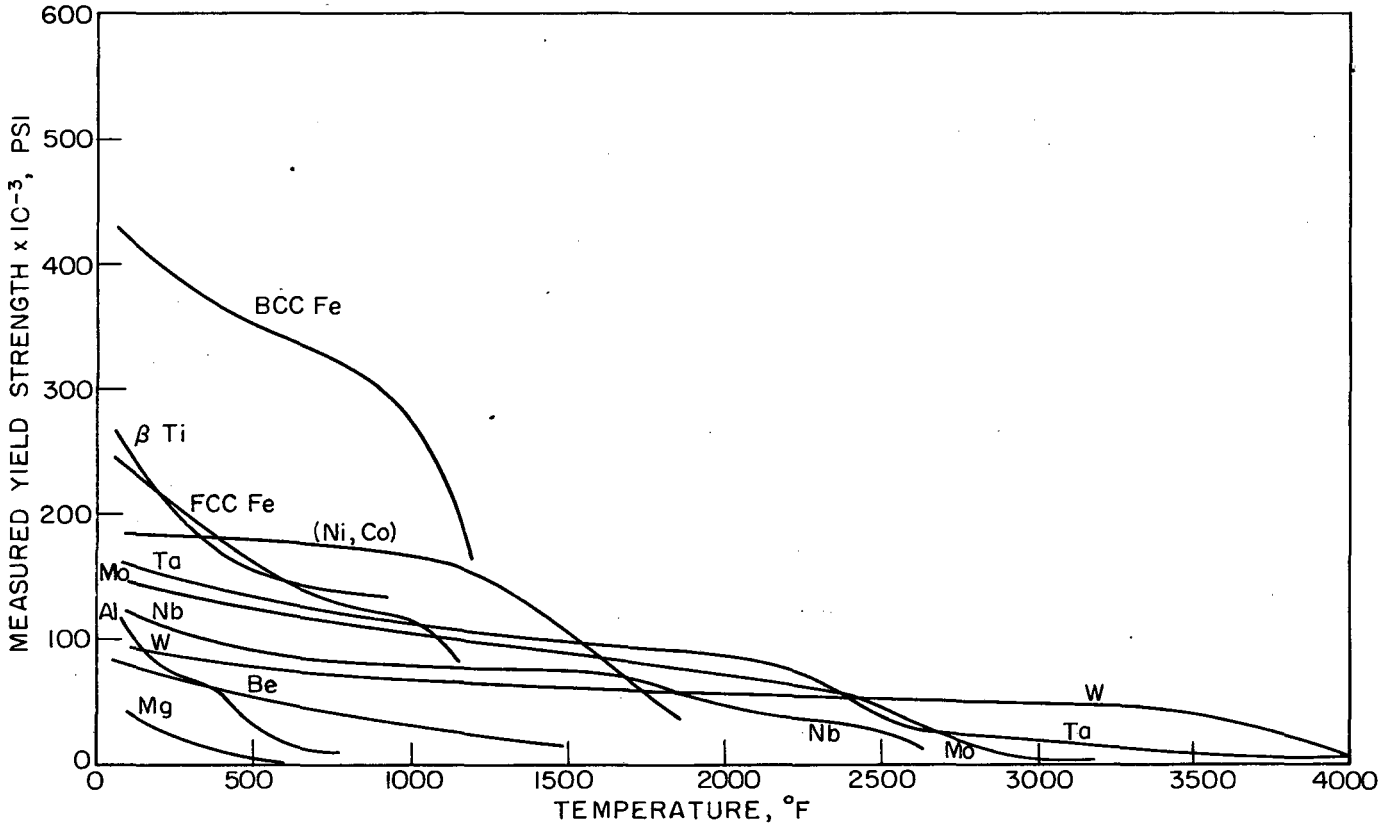

MUB-3083

Fig. 1.

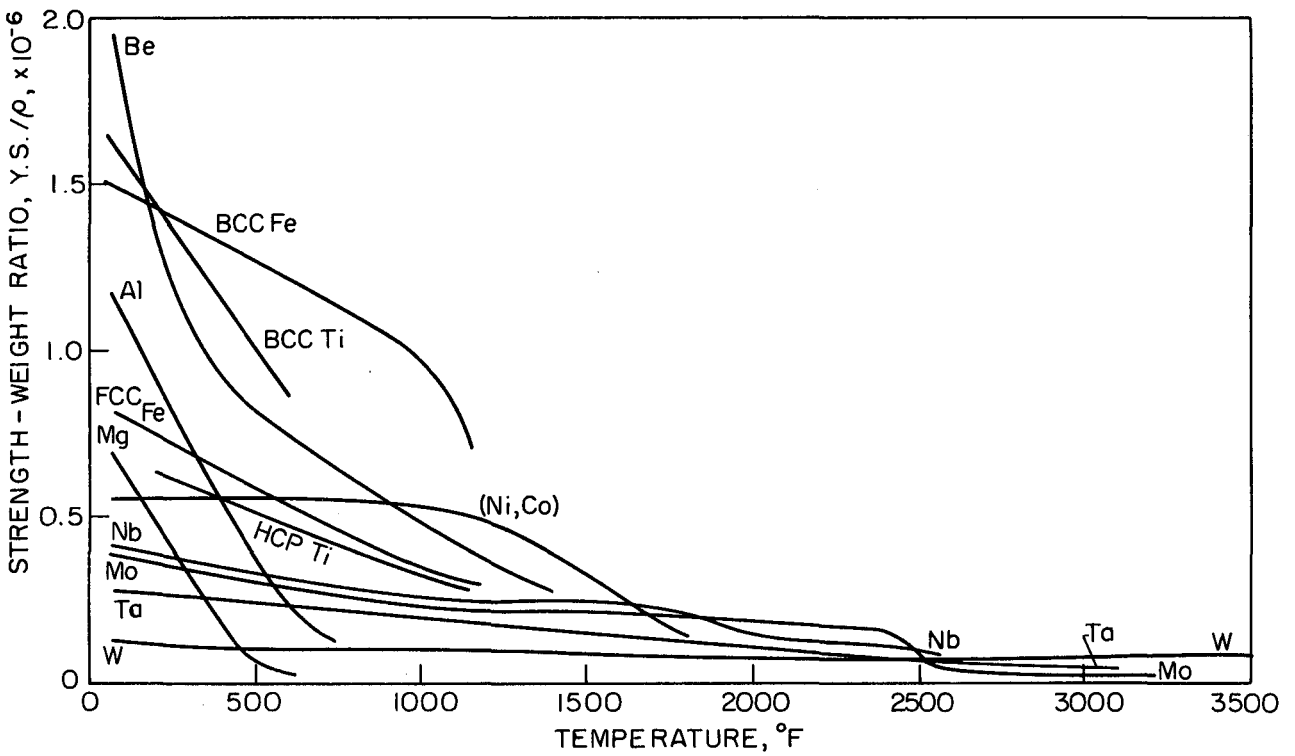

MUB-3080

Fig. 2.

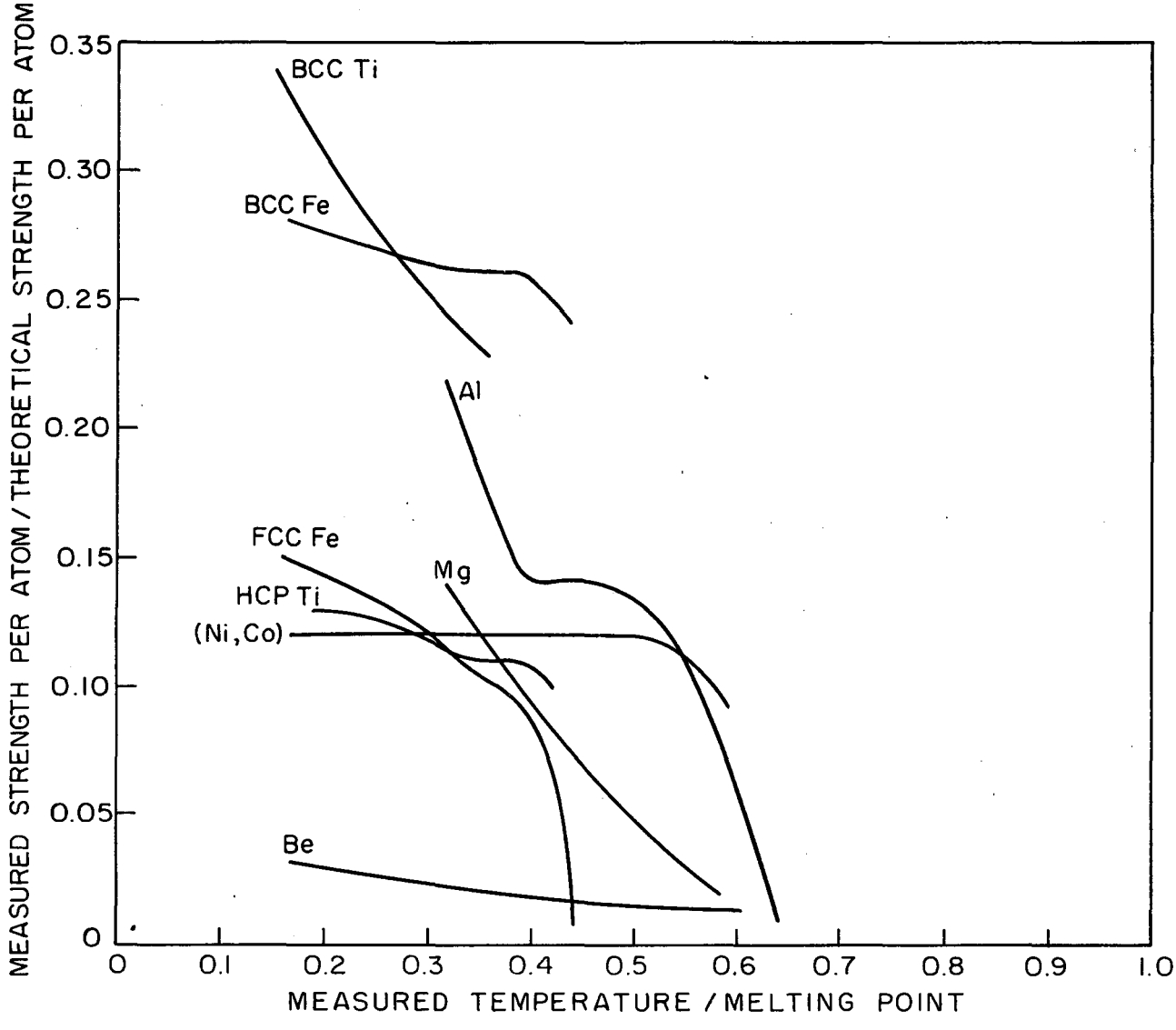

MUB-3075

Fig. 3.

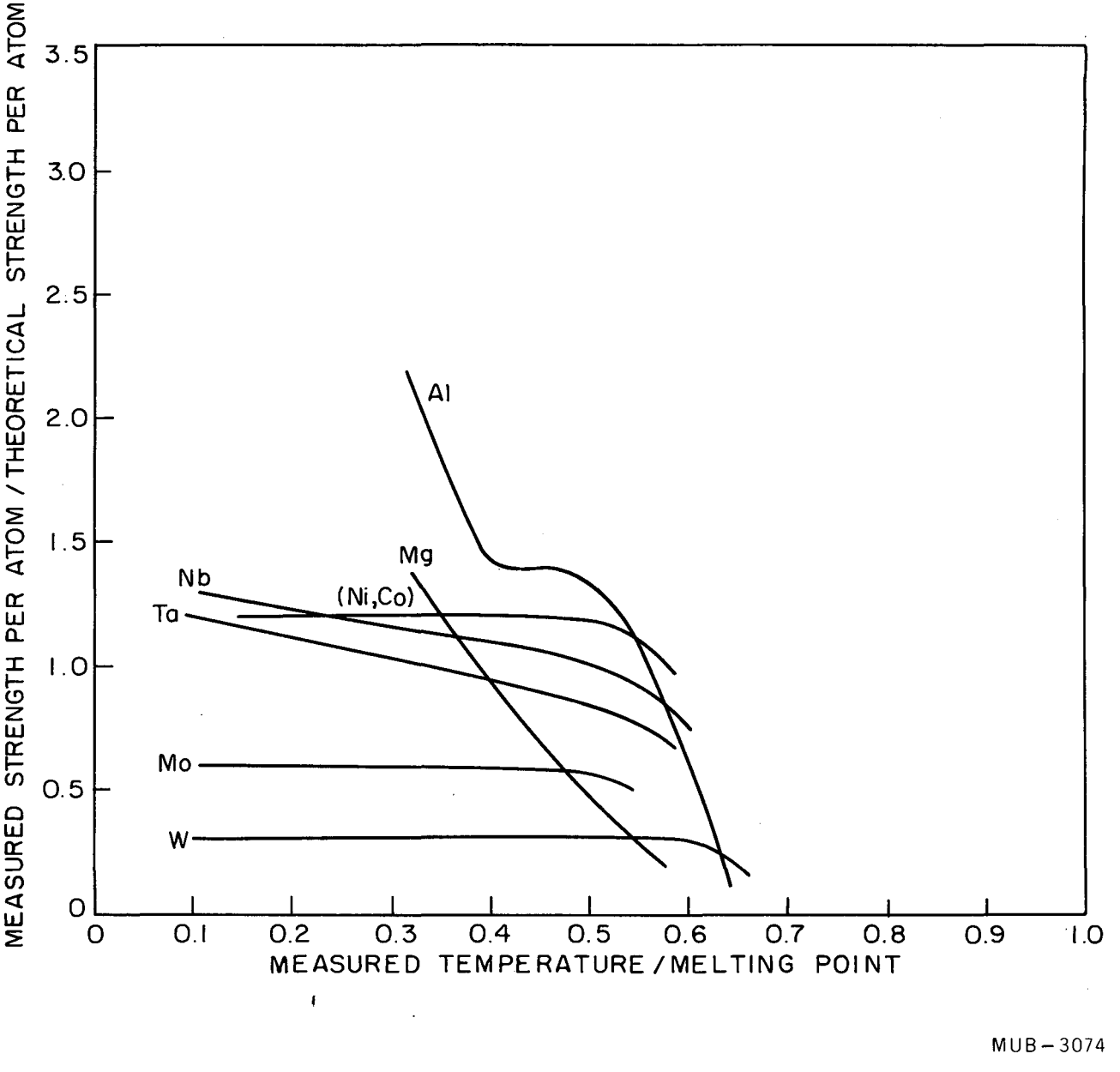
MEASURED STRENGTH PER ATOM / THEORETICAL STRENGTH PER ATOM
3.5
3.0
2.5
2.0
1.5
1.0
0.5
0
0
0.1
0.2
0.3
0.4
0.5
0.6
0.7
0.8
0.9
1.0
MEASURED TEMPERATURE / MELTING POINT
Al
Mg
Nb
(Ni,Co)
Ta
Mo
W
MUB-3074

Fig. 4.

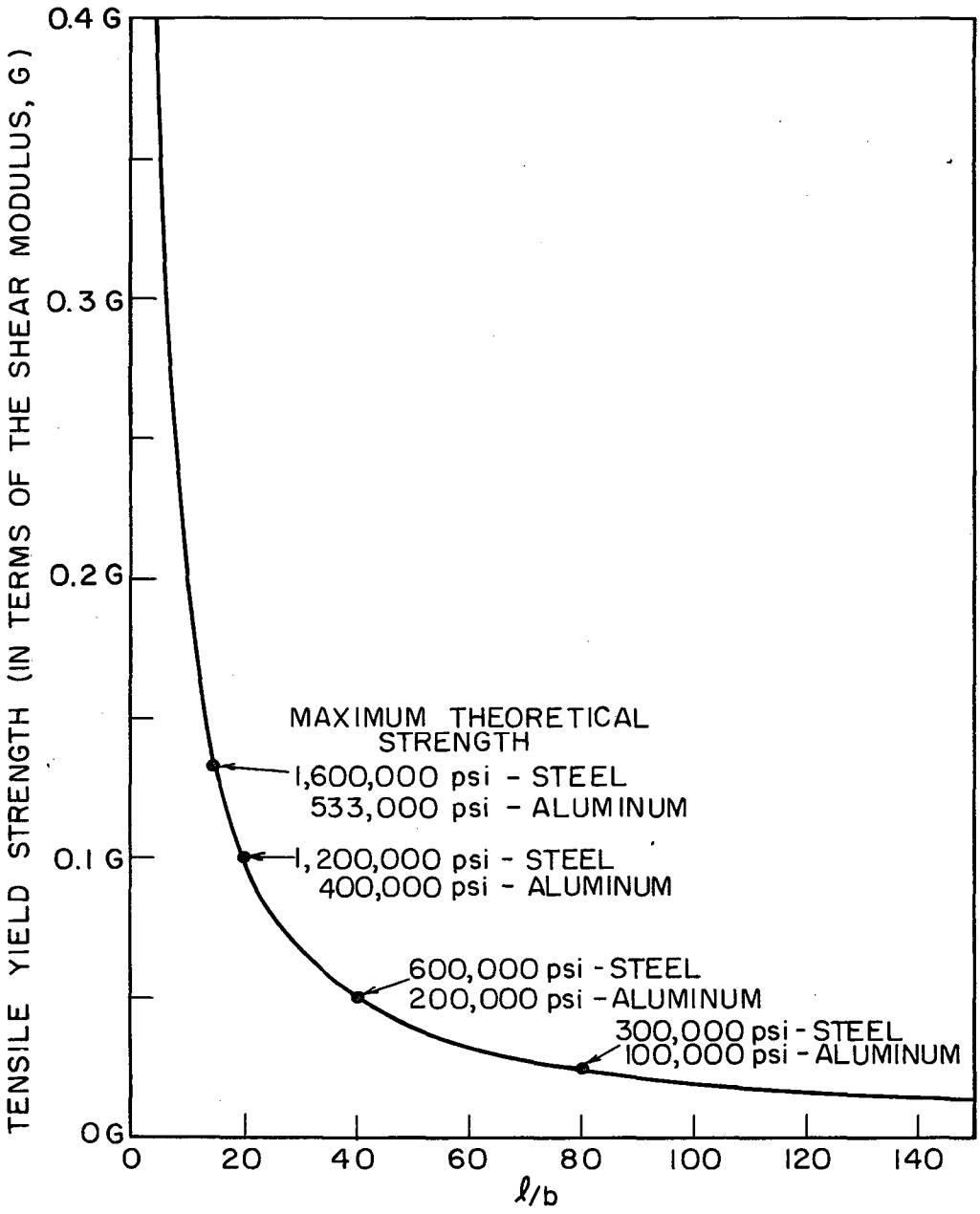
TENSILE YIELD STRENGTH (IN TERMS OF THE SHEAR MODULUS, G)
0.4 G
0.3 G
0.2 G
0.1 G
0 G
0
20
40
60
80
100
120
140
l/b
MAXIMUM THEORETICAL STRENGTH
1,600,000 psi - STEEL
533,000 psi - ALUMINUM
1,200,000 psi - STEEL
400,000 psi - ALUMINUM
600,000 psi - STEEL
200,000 psi - ALUMINUM
300,000 psi - STEEL
100,000 psi - ALUMINUM
MUB - 3072

Fig. 5.

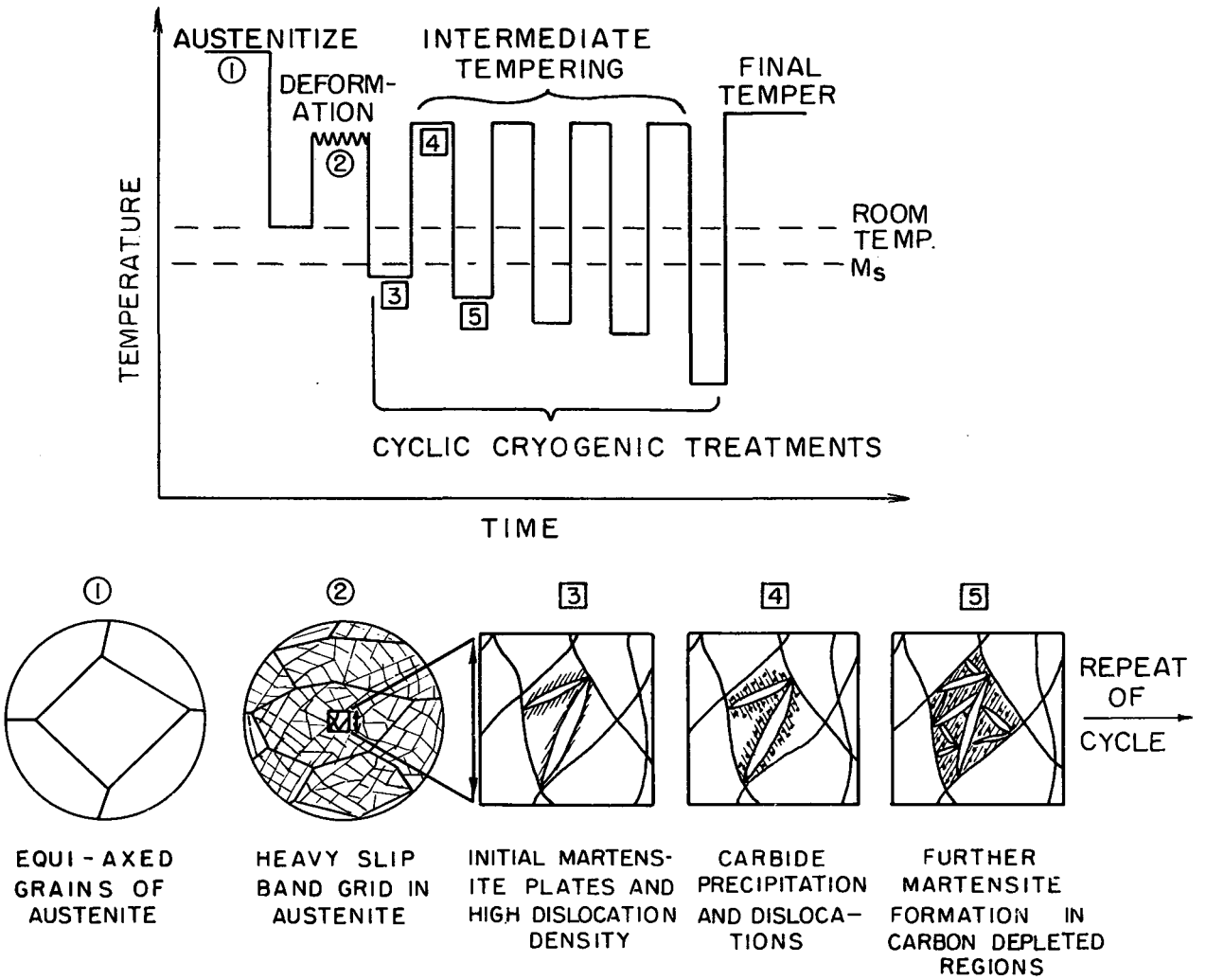
AUSTENITIZE
①
DEFORM-
ATION
②
INTERMEDIATE
TEMPERING
FINAL
TEMPER
4
3
5
ROOM
TEMP.
Ms
TEMPERATURE
CYCLIC CRYOGENIC TREATMENTS
TIME
①
②
3
4
5
REPEAT
OF
CYCLE
EQUI-AXED
GRAINS OF
AUSTENITE
HEAVY SLIP
BAND GRID IN
AUSTENITE
INITIAL MARTENS-
ITE PLATES AND
HIGH DISLOCATION
DENSITY
CARBIDE
PRECIPITATION
AND DISLOCA-
TIONS
FURTHER
MARTENSITE
FORMATION IN
CARBON DEPLETED
REGIONS
MUB-3063

Fig. 6.

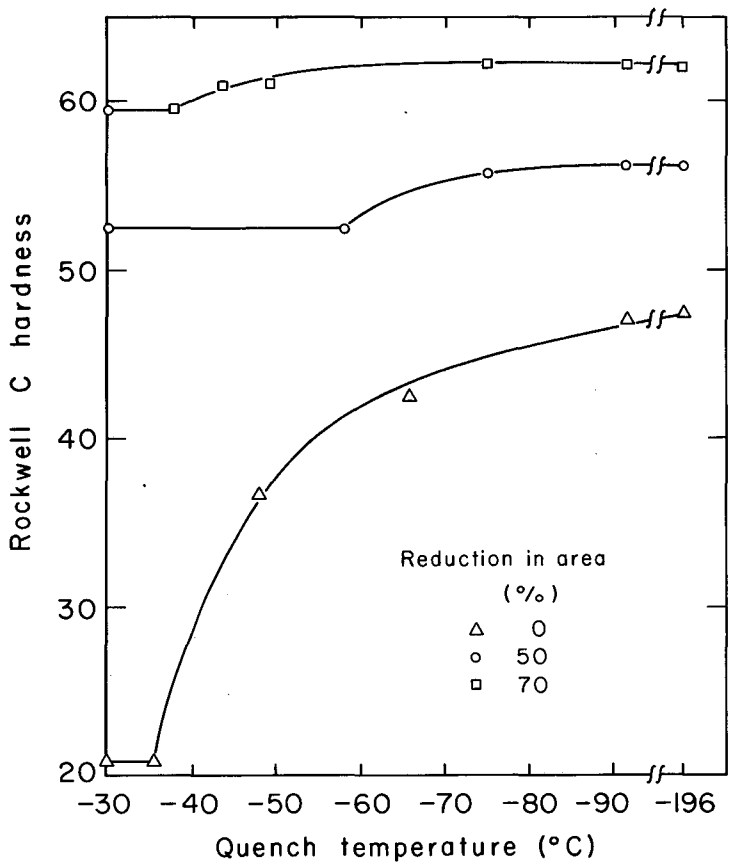
Rockwell C hardness
60
50
40
30
20
-30 -40 -50 -60 -70 -80 -90 -196
Quench temperature (°C)
Reduction in area
(%)
△ 0
○ 50
□ 70
MU-34041

Fig. 7.

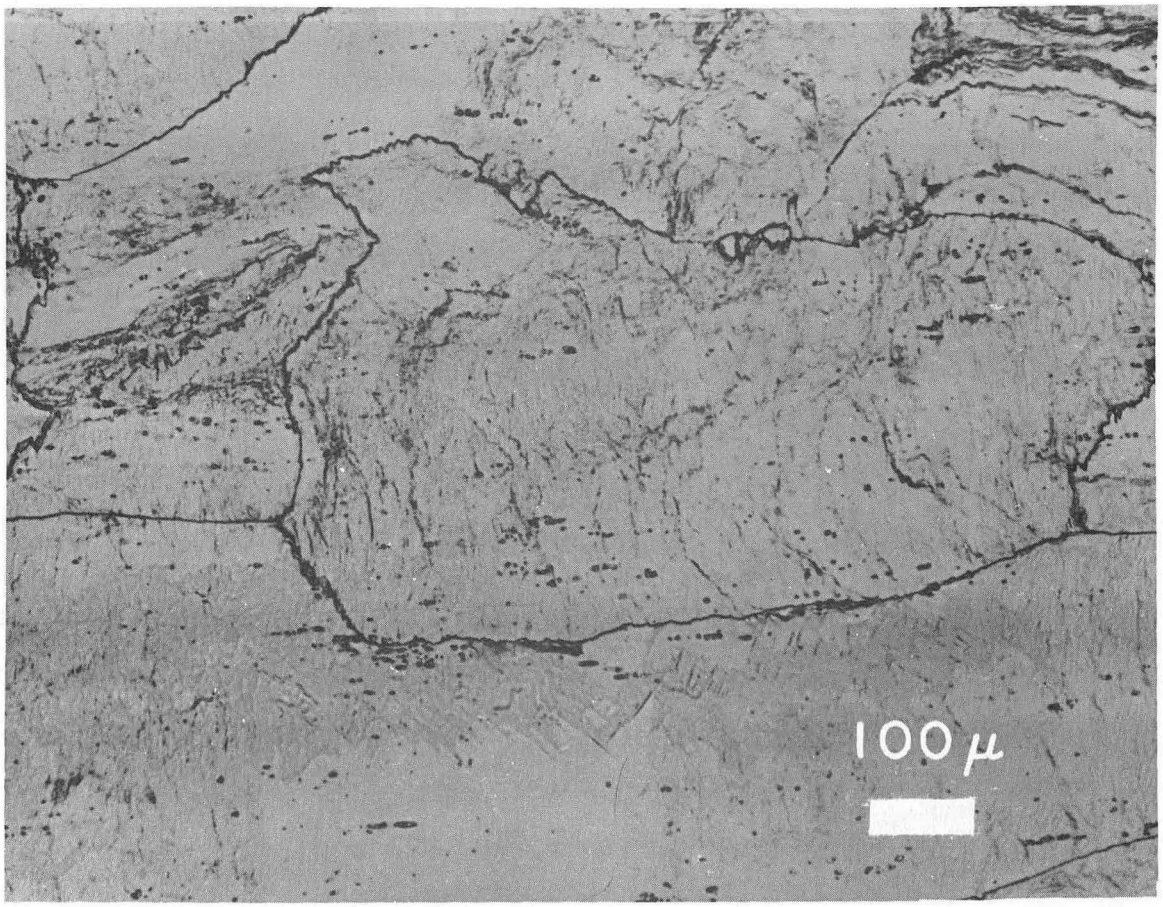

ZN-4434

Fig. 8.

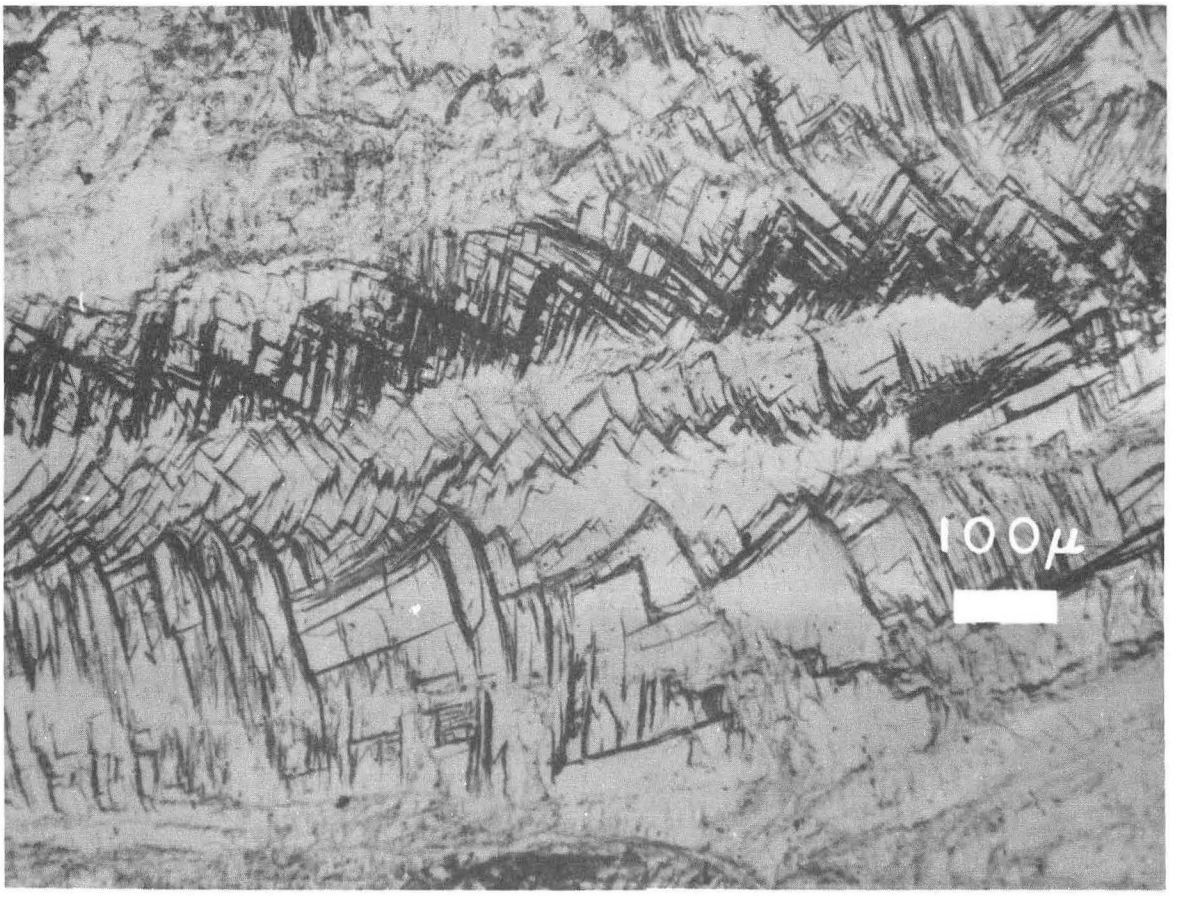

ZN-4311

Fig. 9

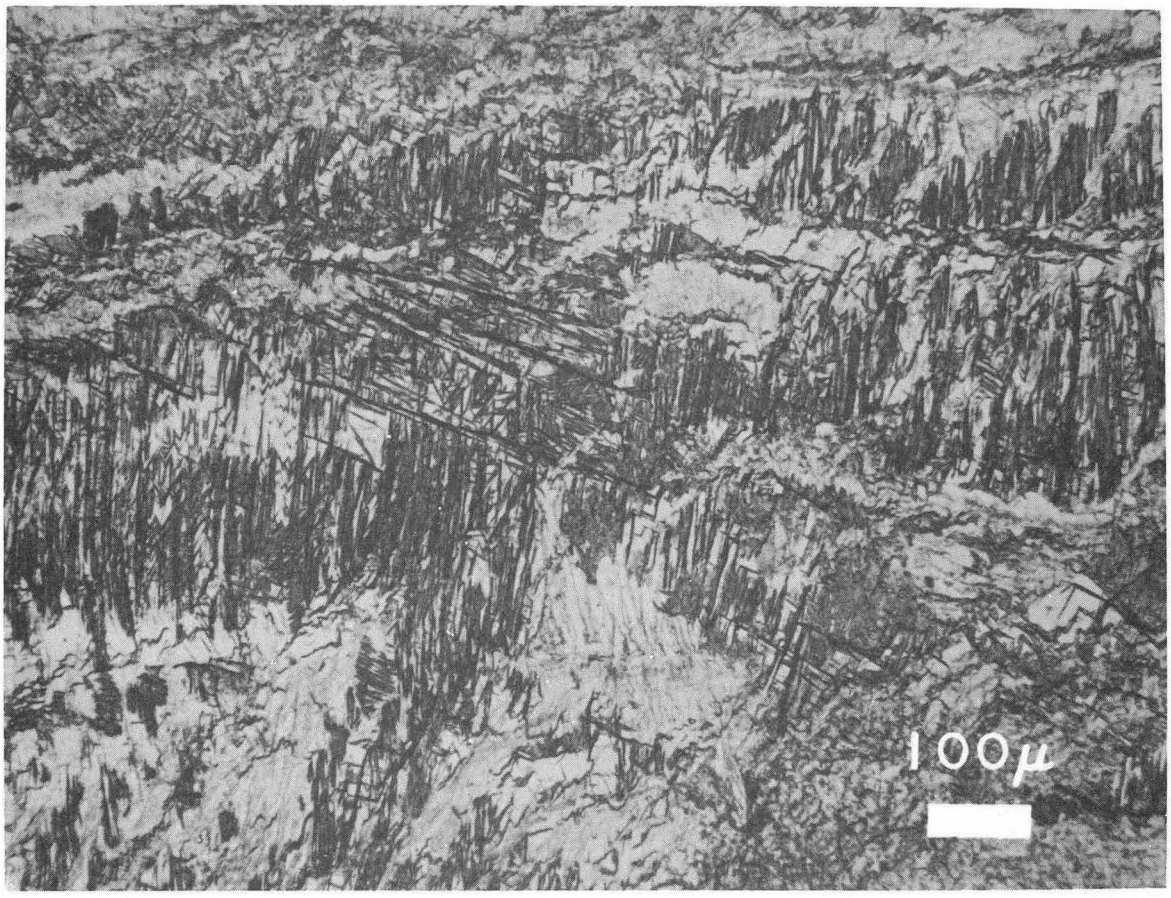

ZN-4314

Fig. 10.

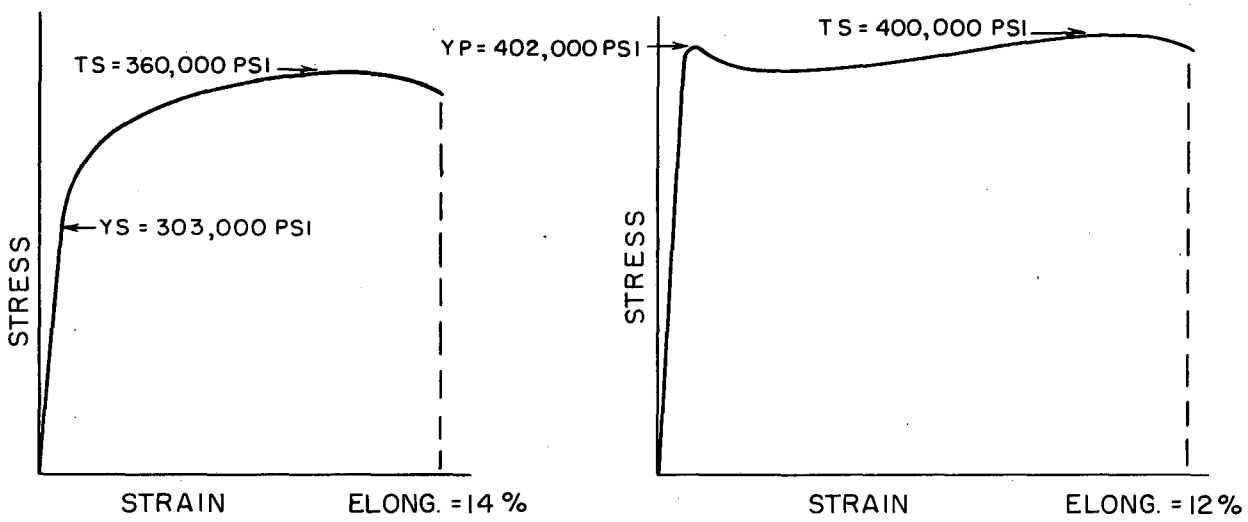

AUSFORMED H-11 STEEL DEFORMED 80%, QUENCHED AND TEMPERED AT 600°F TESTED AT 70°F.

AUSFORMED H-11 STEEL DEFORMED 80 %, QUENCHED AND TEMPERED AT 600°F, STRAINED 2 % AT 300°F, AGED AT 600°F, TESTED AT 70°F.

MUB-3065

Fig. 11.

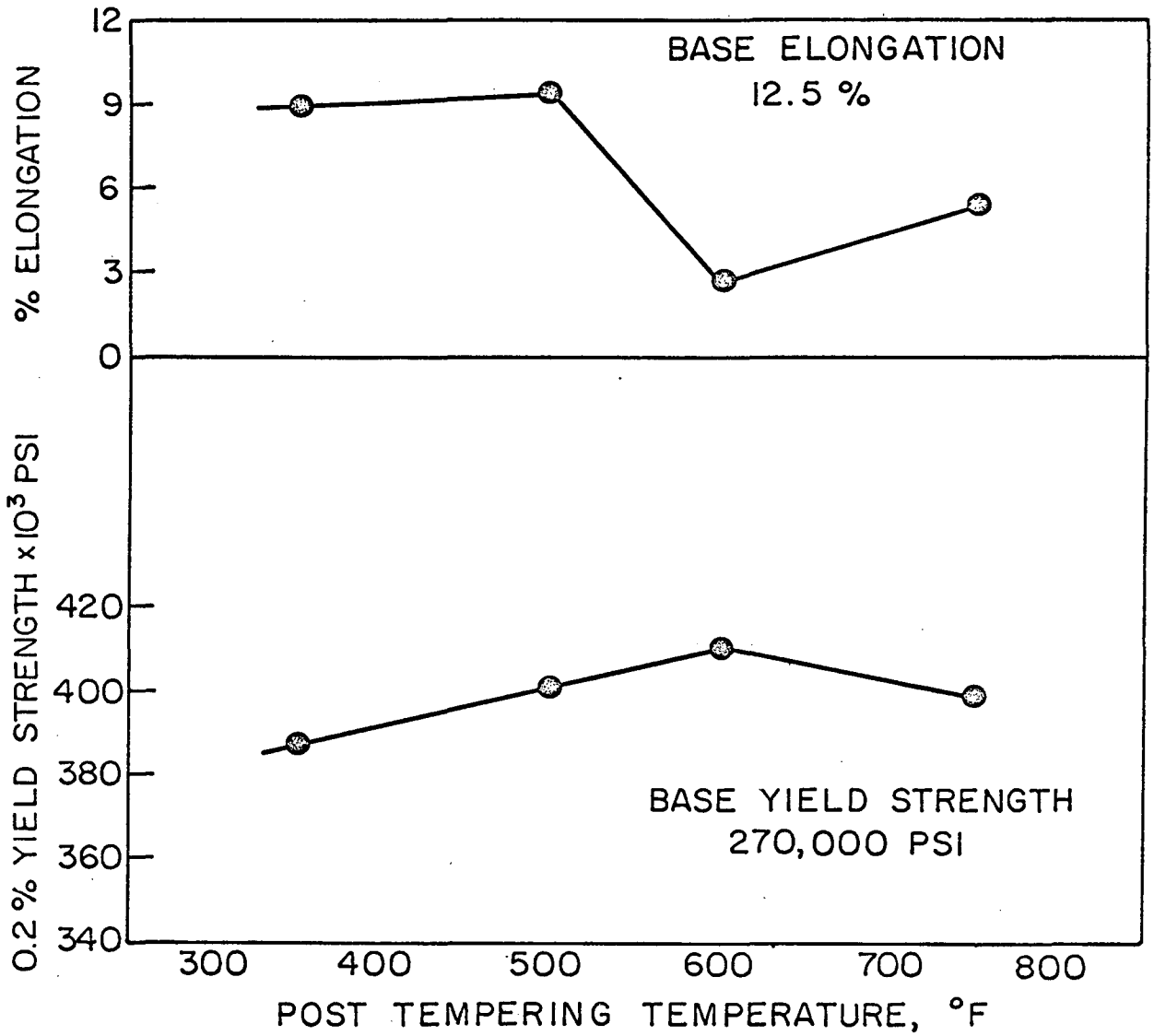

MUB-4096

Fig. 12.

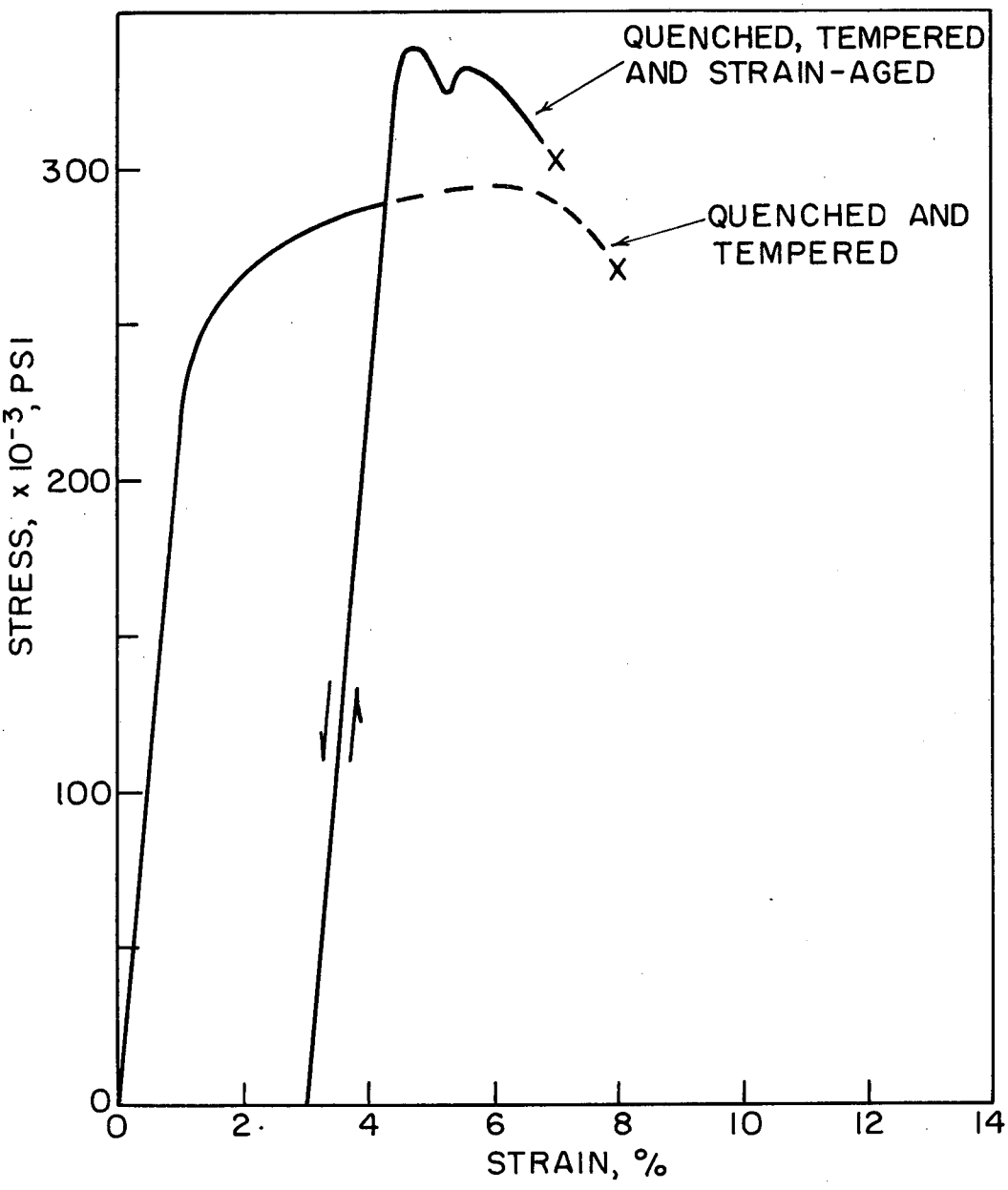
QUENCHED, TEMPERED
AND STRAIN-AGED
QUENCHED AND
TEMPERED
X
X
300
200
100
0
STRESS, x 10⁻³, PSI
0
2
4
6
8
10
12
14
STRAIN, %
MUB-3073

Fig. 13.

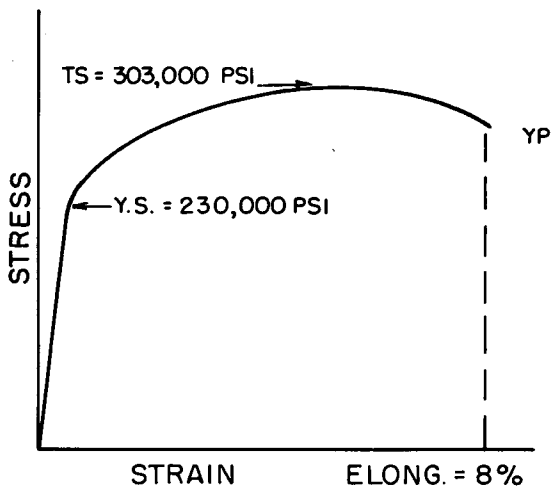

H-11 STEEL QUENCHED AND TEMPERED AT 900°F, TESTED AT 70°F.

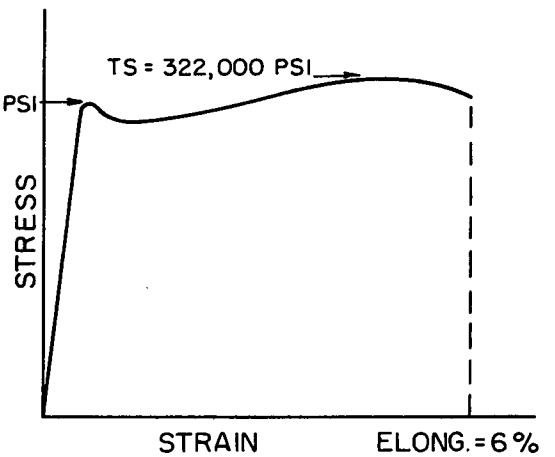

H-11 STEEL QUENCHED AND TEMPERED AT 900°F, STRAINED 2% AT 700°F, AGED AT 900°F, TESTED AT 70°F.

MUB-3067

Fig. 14.

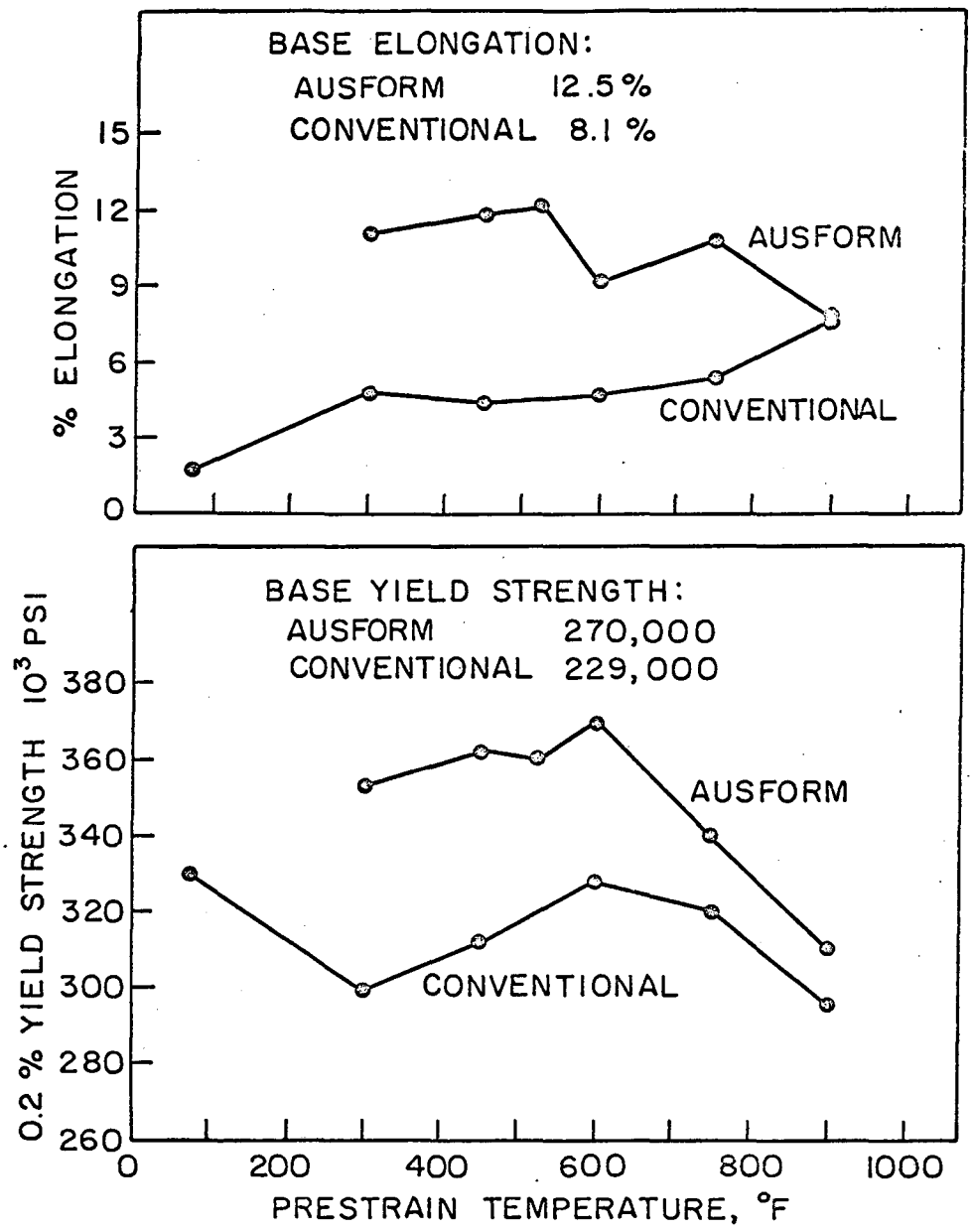
BASE ELONGATION:
AUSFORM 12.5%
CONVENTIONAL 8.1 %
% ELONGATION
15
12
9
6
3
0
AUSFORM
CONVENTIONAL
BASE YIELD STRENGTH:
AUSFORM 270,000
CONVENTIONAL 229,000
0.2 % YIELD STRENGTH 10^3 PSI
380
360
340
320
300
280
260
AUSFORM
CONVENTIONAL
0
200
400
600
800
1000
PRESTRAIN TEMPERATURE, °F
MUB-4097

Fig. 15.

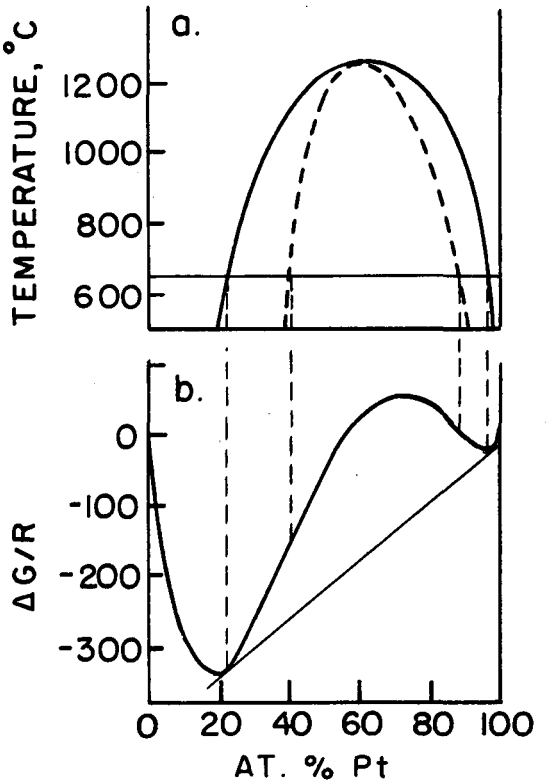

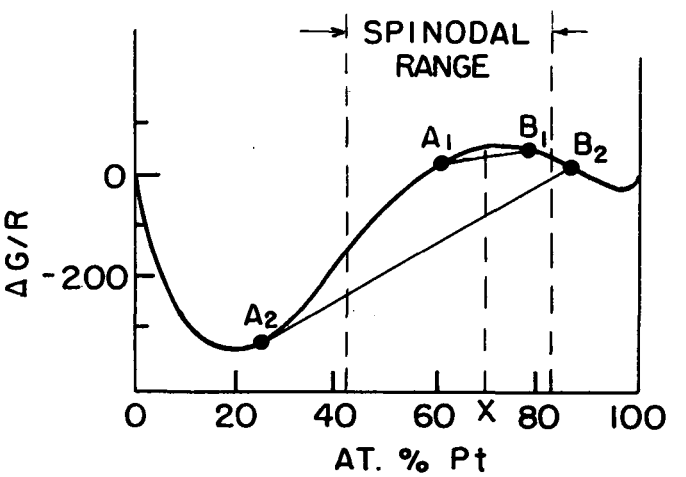

MUB-3062

Fig. 16.

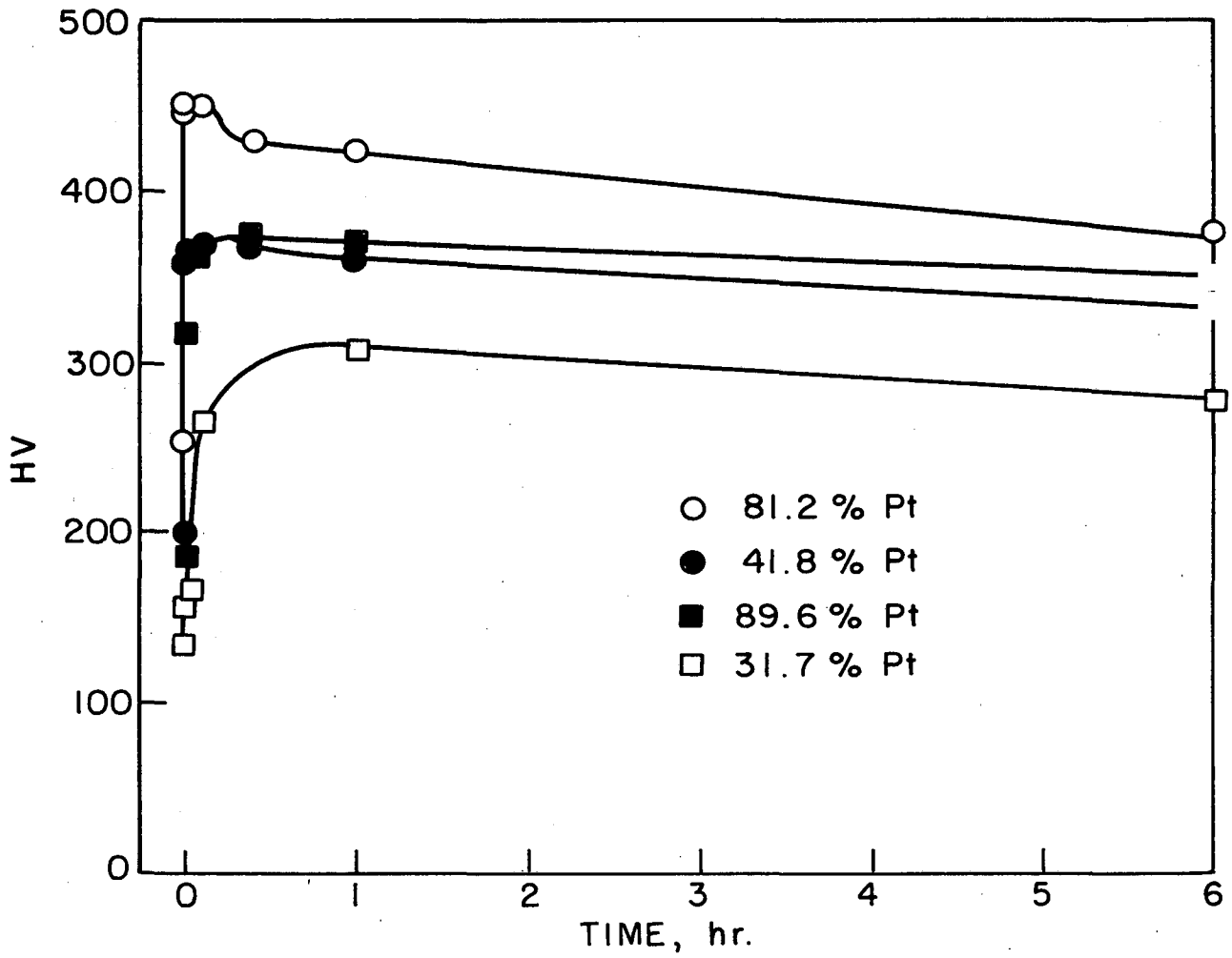

MUB-3064

Fig. 17.

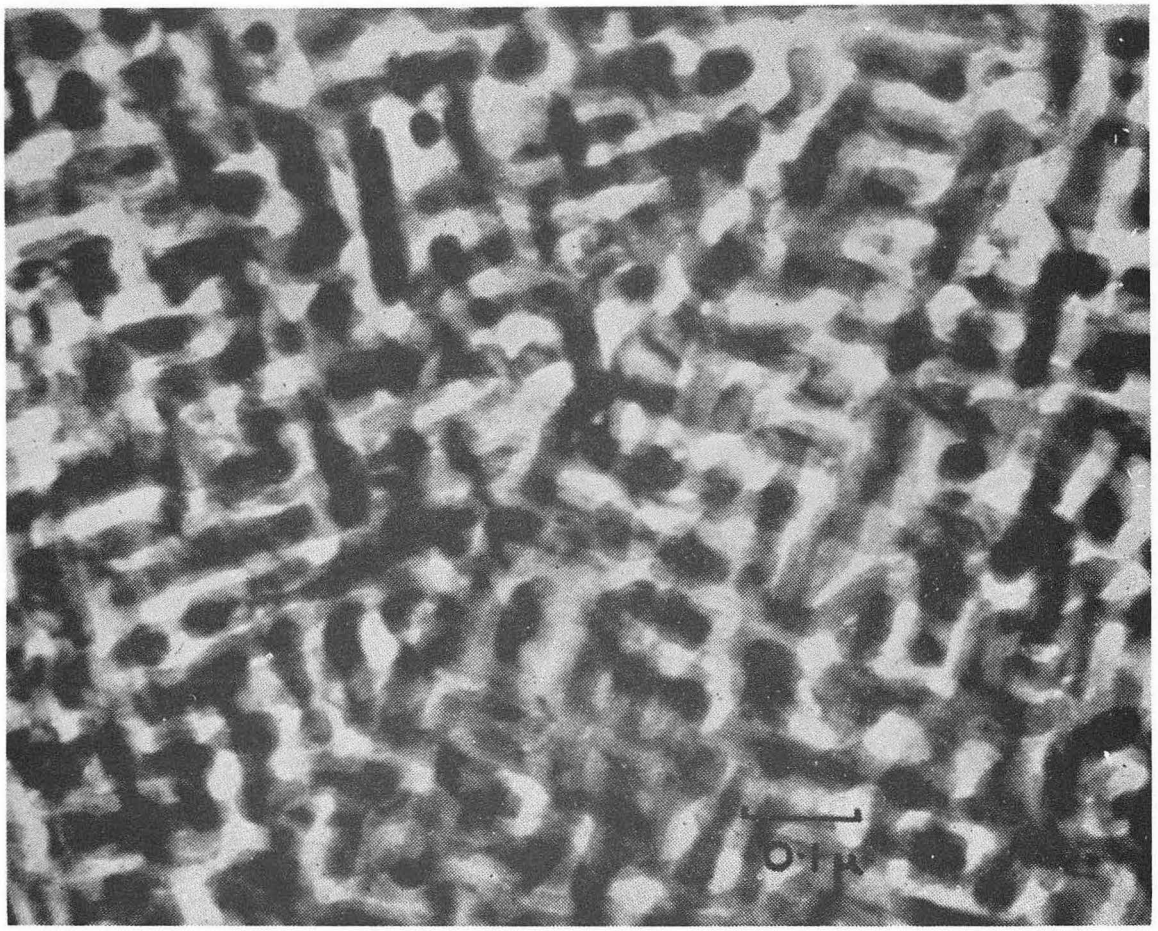

ZN-4436

Fig. 18.

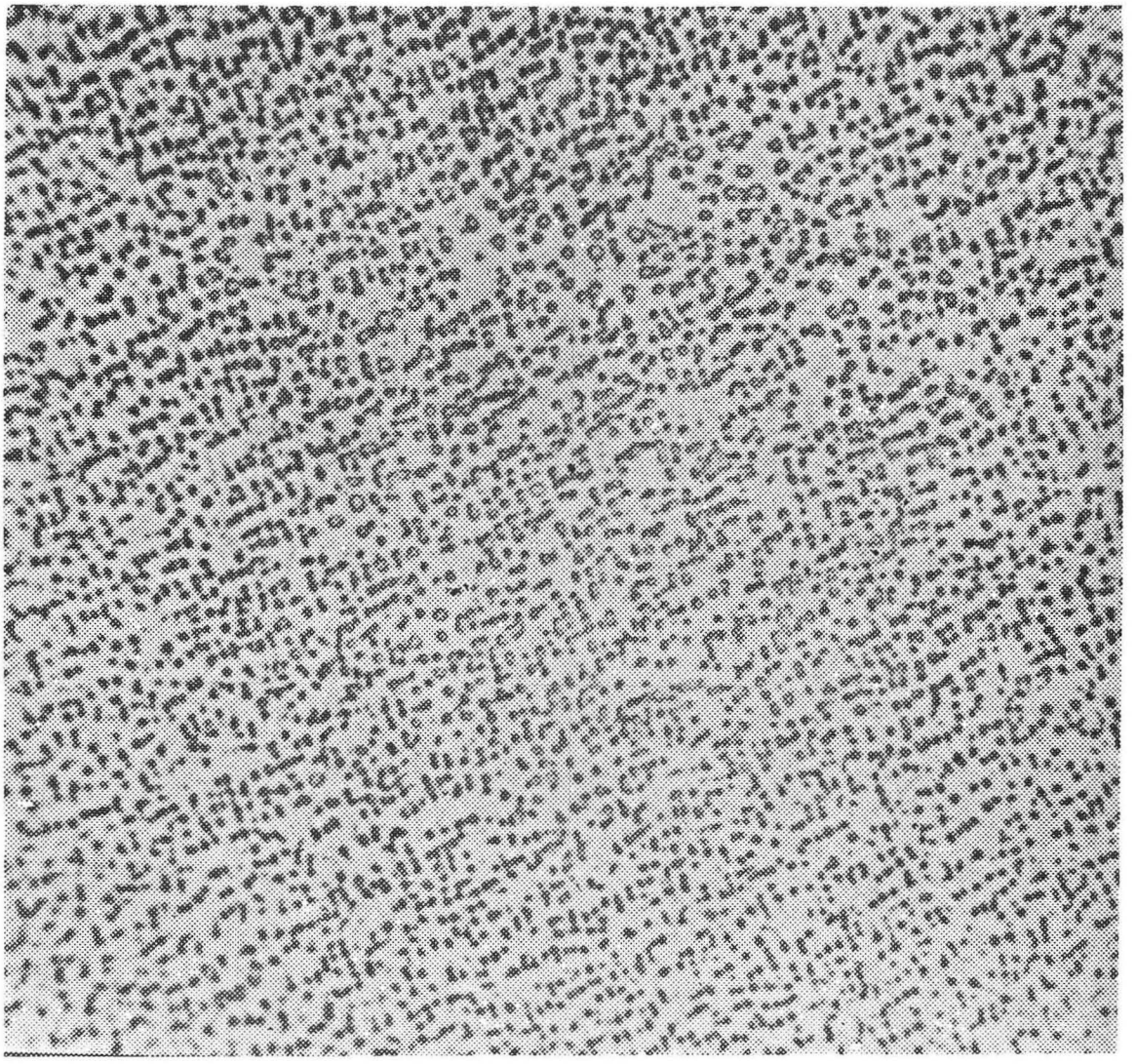

ZN-4435

Fig. 19.

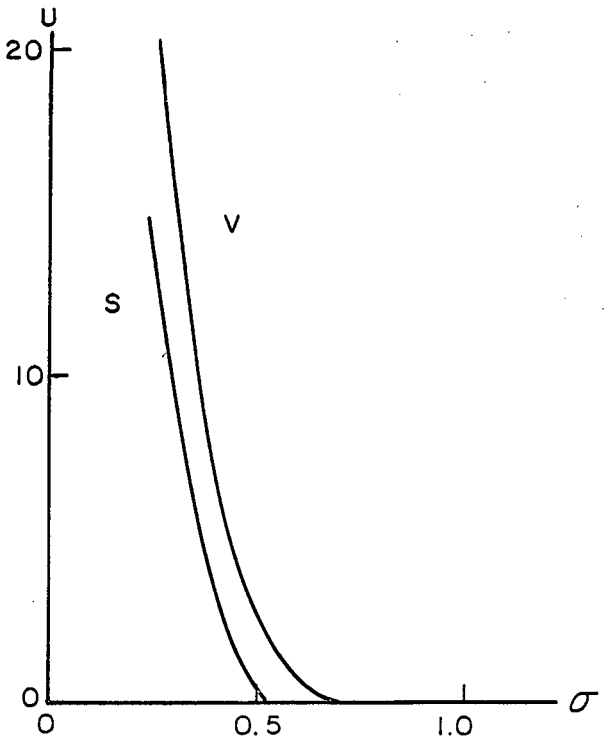

FIG. 1

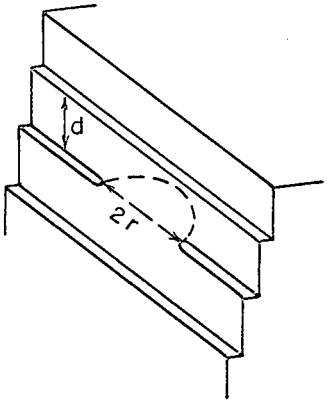

FIG. 2

MUB-4098

Appendix Figs. 1 and 2